A Generalised Methodology for Analytic Construction of 1:1 Resonances around Irregular Bodies: Application to the asteroid Ryugu's Ejecta Dynamics

Stefania Soldini[a,*], Saiki Takanao[b], Hitoshi Ikeda[b], Koji Wada[c], Tsuda Yuichi[b], Naru Hirata[d], Naoyuki Hirata,[e]

[a] *ISAS/JAXA, Sagamihara, Kanagawa 252-5210, Japan. Currently, University of Liverpool, Liverpool L3 5TQ, United Kingdom*
[b] *ISAS/JAXA, Sagamihara, Kanagawa 252-5210, Japan*
[c] *Planetary Exploration Research Center, Chiba Institute of Technology 275-0016, Japan*
[d] *The University of Aizu, Aizu-Wakamatsu 965-8580, Japan*
[e] *Kobe University, Kobe 657-8501, Japan*

Abstract

An analytic construction of 1:1 resonances around irregular bodies is here investigated. A SPH-Mas based gravity model allows a semi-analytic expression of the linearised equations around the equilibrium points. Depending on the sphere packing distribution, the SPH-Mas model can retrieve the same dynamical objects common to others gravity models (i.e. spherical harmonics and polyhedron) or for non uniform density objects. This model has the advantage to define the same particles mesh distribution for both astrophysical and astrodynamics tools and it is computationally optimised for Matlab. The Hayabusa2's Small Carry-on Impactor operation is used as a scenario to study the ejecta particle dynamics around an irregular body. The goNEAR tool was used to simulate the impact operation in a non-linear sense when the effect of the solar radiation pressure perturbation is taken into account for particles size of 10 cm, 5 cm, 1 cm and 1 mm in diameter.

Keywords: Mascons, Smooth Sphere Particles, 1:1 Resonances, Hayabusa2's Small Carry-on Impactor Operation, Fate of Ejecta

*Corresponding author
Email address: stefania.soldini@liverpool.ac.uk (Stefania Soldini)

1. Introduction

In June 2018, the Japanese Hayabusa2 spacecraft successfully arrived at a C-type asteroid. This date marked the start of a 18 months mission exploration around the asteroid Ryugu [1]. Hayabusa2 mission is currently contributing to answer fundamental questions related to the formation of our solar system and the origin of Life [2]. JAXA's Hayabusa2 and NASA's OSIRIS-REx missions [3] are the only two active sample and return missions to small celestial bodies. After the successful deployment of Minerva-II-1A and -1B rovers [4] and CNES-DLR's MASCOT lander [5] last year, 2019 marks the second exploration phase for the Hayabusa2 mission. This year milestones include the first touchdown operation in February 2019, the Small Carry-on Impactor (SCI) operation in April 2019 [6] and the deployment of the Minerva-II-2 rover in August 2019. Japan has set a new first when the Hayabusa2 spacecraft deployed and activated the explosive SCI to successfully form an artificial crater.

The scope of this article is to study the dynamics around Equilibrium Points (EPs) of irregular bodies with application to the asteroid Ryugu. Understanding the natural dynamics around an irregular shape body is a necessary first step to understand for example (1) the fate of particles ejected into space from asteroids, the so called "ejecta" after artificial (e.g. asteroid Ryugu [6]) or natural (e.g. P/2010 A2 [7]) impact events and (2) the fate of ejecta from "active" asteroids (e.g. asteroid Bennu [8]). To the core of our study, we aim to gain a general insights on the dynamics around irregular shape bodies. Moreover, we are looking into a generalised gravity model of celestial bodies that can be easily extended not only to any irregular shape bodies but also to arbitrary density distributions inside the bodies. The selected generalised gravity model should provide a mass distribution that can be used for both hydrodynamics impact simulations and orbital dynamics around EPs.

To study the dynamics around EPs of irregular shape bodies, different approaches have been proposed in literature and three gravity models [9] have been extensively used by several authors:

(a) The spherical harmonics model and its second order approximation (tri-axial ellipsoid) have been studied [10, 11, 12, 13]. For the homogeneous tri-axial ellipsoid, Lara and Elipe [11] and Feng and Hou [12] derived the semi-analytic linear solution around EPs. An analytic solution was derived for inhomogeneous bodies by Ceccaroni and Biggs [13].

(b) The polyhedron model is a high-order fidelity gravity model for uniform density asteroids developed by Werner and Scheeres [14]. A generalised linear analysis around EPs for the polyhedron model has been carried out in [15]. However, the coefficients are not an explicit function of the polyhedron's properties (density, edges and facets).

(c) The multi-point mass [16] or mass cluster [9] or mascons ("mas"s "con" centrations) [17] has been mainly used for explaining the Lunar gravity anomalies [17] originally detected in 1968. In literature, the same gravity model shares different names therefore, in this paper, we will refer from now on to Mascons model. Conversely, Smooth Particles Hydrodynamics (SPH) codes are often used to simulate asteroid impact events [18] and share the problem to handle the transition between a SPH simulation and N-body simulations [19]. Since the SPH and Mascons make use of the same mass conservation law and we are interested to interface the SPH simulations with the N-Body simulations, in this article, we will renamed the selected gravity model as the SPH-Mascons (SPH-Mas) model. The SPH-Mas has been proposed in the past as an interface model between impact physics (SPH simulations) and orbital dynamics (N-Body simulations) to study the ejecta of asteroid (243) Ida [16], however, an analytic expression of the linearised equations was not derived in [16]. Most recent studies on Mascons include the following works [20, 21, 22, 23, 24].

(d) Since the gravity perturbation allows summation of terms, a combination of (a), (b), and (c) models are possible as shown, for the case of Harmonics and Mascons in [25].

When studying the dynamics around asteroids, the (a) and (b) models are widely used. The spherical harmonics and polyhedron model share also some limitations [26]. The harmonics give a global information about the asteroid

gravity but they fail to provide a good representation of the gravity inside the Brillouin sphere. Conversely, the polyhedron model gives a precise solution inside the Brillouin sphere but it experiences information loss at higher altitude [26]. The polyhedron model assumes uniform density and it requires to evaluate the gravity field even in local areas, that is computationally inefficient for our purposes. We understood that the SPH-Mas model has the advantage of allowing to write a semi-analytic expression of the linearised equations of motion around EPs. Those linear equations are derived, in this paper, for the first time. We follow a numerical expansion similar to the well-known linear approximation around the EPs of the restricted three body problem [27] but following the methodology presented in Soldini et al [28]. The coefficients of the derived linear equations are a function of the mass distribution (density) and coordinates. Therefore, in this paper, only the knowledge of a number of spheres packed inside the polyhedron shape is required to find the 1:1 resonances in a simple and fast manner. This implies that not only the methodology has been generalised for any irregular shape body but also for any particular density distribution.

The question now would be: *what is the best SPH-Mas sphere packing representative of the mass distribution of an irregular shape body?*

Although the study of the SPH-Mas sphere packing is out of the scope of this paper, we demonstrated and outline few suggestions when choosing how to pack SPH-Mas spheres within an irregular polyhedron shape. For the scope of demonstrating the validity of our method, we selected a shape model of Ryugu [1] and assumed uniform density. In this case, we aim to use the polyhedron gravity model (or alternatively the spherical harmonics can be used) as our reference model and find an SPH-Mas distribution capable to reproduce the gravity field of the polyhedron and its dynamical objects (EPs and POs). We noticed for example that a uniform distribution even when for 1.4 million masses are used. The implication of this result is in choosing a distribution that is compatible between hydrocodes and astrodynamics codes to correctly make use of the output of the impact physics simulation as input to the N-body planetary equations [18]. Therefore, it is fundamental that the SPH packing can be related

to the overall gravity properties of the asteroid as suggested in this paper.

Finally, the Hayabusa2's Small Carry-on Impactor scenario was selected and a high-fidelity N-Body code (goNEAR) was used to predict the ejecta particle dynamics under effect of solar radiation pressure. Four size of particles (10 cm, 5 cm, 1 cm and 1 mm in diameter) were selected to verify whether ejecta can be temporary capture into Ryugu orbit and pose a treat to the spacecraft. The paper is organised as follow: in Section2 the SPH-Mas gravity model is presented with attention to sphere packing, Section 3 shows the equations of motion and the algebraic equilibrium point equations. In Section (4), we derive the linear equations for the generalised case of irregular shape and non-uniform density asteroids. The application to Ryugu case of the semi-analytic formula is given in Section (5). The results of goNEAR for the SCI impact scenario are presented in Section (6).

2. SPH-Mas Gravity Model

Quantity	Definition	Value
N_f	Polyhedron's Number of Faces	6144
N_e	Polyhedron's Number of Edges	9216
T_B $[h]$	Rotation Period [1]	7.6326
ω $[rad\ s^{-1}]$	Angular Velocity $\left(\frac{2\pi}{T_B\ 3600}\right)$	2.2867×10^{-4}
V_B $[km^3]$	Volume from Polyhedron shape	0.378
ρ_B $[kg\ km^{-3}]$	Density [1]	1.1907×10^{12}
m_B $[kg]$	Mass ($\rho_B\ V_B$)	4.4975×10^{11}
μ $[km^3\ s^{-2}]$	Gravitational Parameter ($G\ m_B$)	3×10^{-8}
r_B $[km]$	Equivalent Radius	0.448442

Table 1: Asteroid Ryugu's Properties.

In this article, the gravity of an irregular shape body is modeled with a cluster of spheres, SPH-Mas. Each spherical particle contribute in the overall gravity field of the body. The exterior gravity potential of each sphere behaves

as a single point mass. The potential of the irregular body is the result of the summation of each point mass's potential that contributes to the overall potential field such that:

$$U_{sph} = \sum_{i\,=\,1}^{N_{sph}} \left(\frac{Gm_i}{|\boldsymbol{r} - \boldsymbol{r}_i|} \right), \tag{1}$$

where m_i $(i = 1, \ldots, N_{sph})$ is the mass of each SPH-Mas for a total of N_{sph} masses. $\boldsymbol{r}$ is the distance from the field point and the center of the reference frame (centered in the center of mass of the asteroid) as shown in Fig. (3). $\boldsymbol{r}_i$ is the distance of each masses with respect to the center of the reference frame as shown in Fig. (3). The total mass of the asteroid is conserved and given by:

$$m_b = \sum_{i\,=\,1}^{N_{sph}} m_i. \tag{2}$$

For the SPH-Mas model, the gradient of U is simply given by:

$$\boldsymbol{\nabla} U_{sph} = -\sum_{i\,=\,1}^{N_{sph}} \left(\frac{Gm_i}{|\boldsymbol{r} - \boldsymbol{r}_i|^3} \begin{Bmatrix} X - X_i \\ Y - Y_i \\ Z - Z_i \end{Bmatrix} \right), \tag{3}$$

where the acceleration of the SPH-Mas gravity model is $\boldsymbol{a}_{sph} = \boldsymbol{\nabla} U_{sph}$. The Laplacian of U_{sph} is given by:

$$\boldsymbol{\nabla}^2 U_{sph} = \sum_{i\,=\,1}^{N_{sph}} \begin{bmatrix} -\frac{Gm_i}{(r-r_i)^3}\left[1 - \frac{3(X-X_i)^2}{(r-r_i)^2}\right] & Gm_i \frac{3(X-X_i)(Y-Y_i)}{(r-r_i)^5} & Gm_i \frac{3(X-X_i)(Z-Z_i)}{(r-r_i)^5} \\ Gm_i \frac{3(X-X_i)(Y-Y_i)}{(r-r_i)^5} & -\frac{Gm_i}{(r-r_i)^3}\left[1 - \frac{3(Y-Y_i)^2}{(r-r_i)^2}\right] & Gm_i \frac{3(Y-Y_i)(Z-Z_i)}{(r-r_i)^5} \\ Gm_i \frac{3(X-X_i)(Z-Z_i)}{(r-r_i)^5} & Gm_i \frac{3(Y-Y_i)(Z-Z_i)}{(r-r_i)^5} & -\frac{Gm_i}{(r-r_i)^3}\left[1 - \frac{3(Z-Z_i)^2}{(r-r_i)^2}\right] \end{bmatrix}. \tag{4}$$

Note that Eq. (1), Eq. (3) and Eq. (4) can be written in a vector form when using Matlab. As previously pointed out by Russel and Arora [25], we can confirm that using Matlab for SPH-Mas allows a fast computation of the gravity field due to the use of Matlab's matrix and vector operations. In Matlab, it is recommended to avoid "for loops" and when possible to use matrix operations for speeding up purposes. In that respect, we noticed that even for 1.4 million masses our "fun_UDUmas.m" is way faster than computing the polyhedron

model [14] also when using the optimised speed .mex file generated with Matlab coder for the polyhedron. This happens because the polyhedron model requires "two for loops" to evaluate the vector field $\boldsymbol{r}$ with respect to each faces and edges. Table 1 show the reference properties of the asteroid Ryugu that are used throughout the paper.

2.1. Packing of Spheres

We consider Ryugu's polyhedron model published in Watanabe et al. [1] as our "high fidelity" gravity model[1]. We distribute the SPH-Mas within the asteroid shape such that we can approximate Ryugu's "high fidelity" gravity field. For the scope of testing our semi-analytic formula, we compared a uniform sphere packing approach with a random packing approach for different numbers of SPH-Mas. Figure 2 shows the comparison between the uniform distribution in the left panel and the random distribution in the right panel for $N_{sph} = 19$, 58, 1,605 and 1,406,146. To construct the uniform sphere packing distribution, we follow the following steps:

- First, we consider a sphere of size slightly bigger than Ryugu such that Ryugu shape is inside the sphere;
- Second, we uniformly distribute points inside the selected sphere and we construct a grid of points by using the function "ball_grid.m" developed by Burkardt [29]. The grid is defined by specifying the radius and the center of the sphere, and the number of subintervals h into which the horizontal radius should be divided. Thus, a value of $h = 2$ will result in 5 points along that horizontal line ($y = 0$) as shown in Fig. 1;

[1] The same approach can be used for the spherical harmonics.

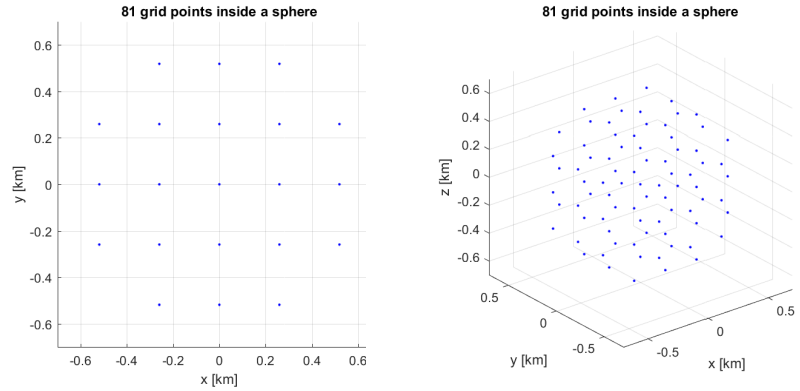

(a) X-Y view. (b) 3D View.

Figure 1: A spherical grid of radius 0.65 km for $h = 2$ results in 81 points inside the sphere.

- Third, we select the SPH-Mas that are inside Ryugus's polyhedron and discard the other points by using the function "inpolyhedron.m" developed by Holcombe [30]. For $h = 2$, the spherical grid has 81 points in which only 19 are inside Ryugus's shape as shown in Fig. 2.a;

- Fourth, we uniformly distribute[2] the overall asteroid mass within the selected SPH-Mas such that Eq. (2) holds true and $m_i = \frac{m_b}{N_{sph}}$. Note that a non uniform density distribution can be easily applied here. Table 2 shows the number of N_{sph} as a function of h for a sphere of radius 0.65 km. The grid resolution and the vale of each mass, m_i, is also listed.

For the case of random sphere packing, the procedure is simpler. We consider a random number of points within the Ryugu's polyehdron. We presented two possible sphere packing approaches where our analysis turns to be sufficient for the scope of this paper. Further studies on sphere packing should be investigated in future works. Examples of possible sphere packing can be found in literature and we refer to the work of other authors [20, 21, 24, 18, 23, 22].

[2]Note that a non-uniform density distribution is also possible.

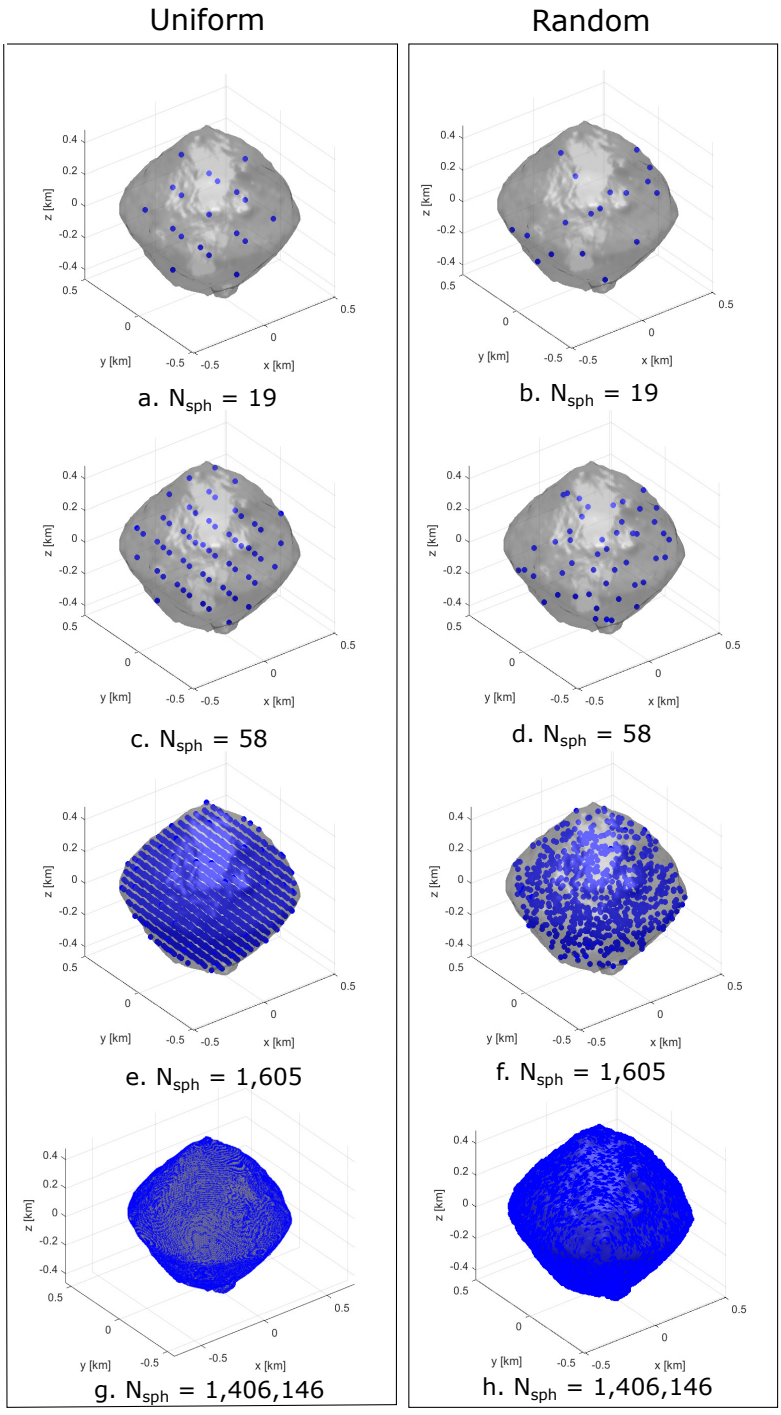

Figure 2: Examples of SPH-Mascons packing inside the Ryugu's polyhedron shape. A comparison between the uniform and random packing for N_{sph} = 19, 58, 1,605 and 1,406,146.

h	Grid Res. [m]	N_{grid}	N_{sph}	$m_i \times 10^7$ [kg]
2	259.37	81	19	2,367.11
3	185.27	179	58	775.43
10	61.75	4,945	1,605	28.022
50	7.96	540,113	178,415	0.25
100	4	4,252,701	1,406,146	0.032

Table 2: Uniform sphere packing in a sphere of radius 0.65 km.

3. Equations of Motion

The equations of motion are written in the asteroid fixed rotating frame (marked as FIXED in Fig. 3) and are given by:

$$\begin{cases} \ddot{X} - 2\omega\dot{Y} &= \Omega_x + a_{sx} \\ \ddot{Y} + 2\omega\dot{X} &= \Omega_y + a_{sy} \\ \ddot{Z} &= \Omega_z + a_{sz} \end{cases} \tag{5}$$

where Ω is the effective potential and it is defined as:

$$\Omega = \frac{1}{2}\omega^2(X^2 + Y^2) + U_{sph}, \tag{6}$$

with the angular velocity, ω, defined as in Table 1. The SPH-Mas potential, U_{sph}, is given in Eq. (1). The acceleration of radiation pressure (SRP acceleration), $\boldsymbol{a}_s$ is defined as:

$$\boldsymbol{a}_s = -(1+\rho)P_0\frac{A}{m}\frac{(\boldsymbol{d}-\boldsymbol{r})}{|\boldsymbol{d}-\boldsymbol{r}|^3}, \tag{7}$$

where $\boldsymbol{d}$ and $\boldsymbol{r}$ are the position vectors of the Sun and dust particle respectively from the asteroid center. Note that the position of the Sun is time dependant and the Sun's ephemeries are taken from SPICE Toolkit in J2000 Equatorial (J2000EQ) centered at the Solar System Barycenter (SSB) through the SPICE's "skezer" function. The position of the Sun is then expressed in the

J2000EQ@Ryugu as shown in Fig. 3. The coordinates of the Sun are given in J2000EQ and transformed in asteroid fixed frame though the rotation matrix $\boldsymbol{C}_{J2000toFIXED}$ though the SPICE's "sxform" function.

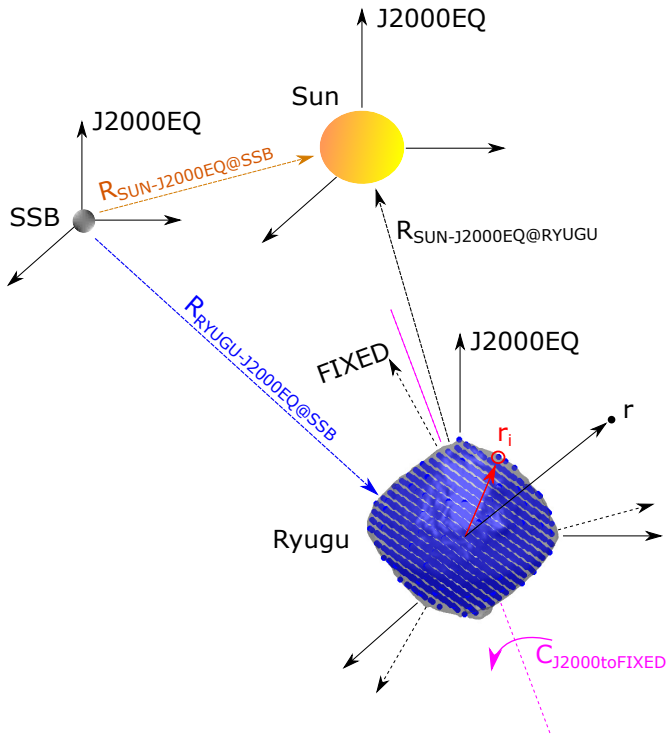

Figure 3: Reference frames: J2000EQ centered at Solar System Barycenter (J2000EQ@SSB), at the Sun (J2000EQ@SUN) and at Ryugu (J2000EQ@RYUGU) and asteroid fixed (FIXED). The position of the i-SPH-Mas is marked in red, $\boldsymbol{r}_i$ and the position of the vector field in black, r.

3.1. Location of the Equilibrium Points without the effect of SRP

In this section, we compute the location of the equilibrium points when the SRP perturbation is neglected and therefore Eq. (5) is no longer time dependant. Although the computation of the equilibrium points around asteroids is not new, the equation of equilibria for the SPH-mas model, $\boldsymbol{\nabla}\Omega = \boldsymbol{0}$, are a

nonlinear system of algebraic equations that provides the components γ_1, γ_2 and γ_3 for a selected number of SPH-Mas particles, N_{sph}, their coordinates, m_i, and mass distribution, $\boldsymbol{r}_i$:

$$\begin{cases} \omega^2\gamma_1 + \sum\limits_{i\,=\,1}^{N_{sph}} \left[\dfrac{\mu_i(X_i-\gamma_1)}{((X_i-\gamma_1)^2+(Y_i-\gamma_2)^2+(Z_i-\gamma_3)^2)\sqrt{(X_i-\gamma_1)^2+(Y_i-\gamma_2)^2+(Z_i-\gamma_3)^2}} \right] = 0 \\ \omega^2\gamma_2 + \sum\limits_{i\,=\,1}^{N_{sph}} \left[\dfrac{\mu_i(Y_i-\gamma_2)}{((X_i-\gamma_1)^2+(Y_i-\gamma_2)^2+(Z_i-\gamma_3)^2)\sqrt{(X_i-\gamma_1)^2+(Y_i-\gamma_2)^2+(Z_i-\gamma_3)^2}} \right] = 0 \\ \sum\limits_{i\,=\,1}^{N_{sph}} \left[\dfrac{\mu_i(Z_i-\gamma_3)}{((X_i-\gamma_1)^2+(Y_i-\gamma_2)^2+(Z_i-\gamma_3)^2)\sqrt{(X_i-\gamma_1)^2+(Y_i-\gamma_2)^2+(Z_i-\gamma_3)^2}} \right] = 0 \end{cases} \tag{8}$$

An algebraic system of equations for the computation of the equilibrium points' location as a function of the asteroid's mass distribution was not explicitly derived by previous authors. Our formulation holds true in a general sense. From Eq. (8), it is clear that the location of the equilibrium points $\gamma_1(m_i, \boldsymbol{r}_i)$, $\gamma_2(m_i, \boldsymbol{r}_i)$ and $\gamma_3(m_i, \boldsymbol{r}_i)$ is function of the SPH-Mas's masses value, m_i, (or density distribution) and coordinates, $\boldsymbol{r}_i$ and the angular rotation of the asteroid, ω. Regarding the dependency in ω, we recall that the radial distance of the EPs from the center of the asteroid can be approximated for a spherical body as $\sqrt[3]{\frac{\mu}{\omega^2}}$, therefore for fast spinning asteroids the EPs tend to move towards the center of the asteroid. Figure 4 gives a qualitative comparison of the number and locations of the EPs when comparing a uniform and random sphere packing distribution. The curves in Fig. (4) are called Zero Velocity Curves (ZVC) and obtined by fixing a value of the effective potential, $-\Omega$. The coordinates of the EPs shown in Fig. (4) are listed in Table 8 together with the EPs of the polyhedron model with number of faces and edges presented in Table 1. By comparing the uniform sphere packing with the random sphere packing, it is clear that under the assumption of uniform density polyhedron, the uniform sphere packing is preferable to the random sphere packing even for the case of N_{sph} major to the order of million spheres. Indeed, the random sphere packing does not necessarily preserve the geometry of the EPs, it improves its accuracy

when million of spheres are considered; however, it is less accurate than the uniform sphere packing when the same number of spheres is considered as shown in Fig. (4.e-4.f).

N_{sph}	EPs	γ_1 (unf) [m]	γ_1 (rand) [m]	γ_1 (poly) [m]	γ_2 (unf) [m]	γ_2 (rand) [m]	γ_2 (poly) [m]	γ_3 (unf) [m]	γ_3 (rand) [m]	γ_3 (poly) [m]
	EP1	827.4434	838.9311	727.7665	0	-328.5149	409.4026	0	89.0574	-6.5485
	EP2	594.2580	-45.3435	-315.4729	586.5152	765.27954	780.2082	0	1.1505	1.188
	EP3	-2.4819	-869.2943	-832.2260	827.5001	-28.3229	97.9041	0	-41.3317	4.3232
19	EP4	-590.4370	-406.9261	-370.5562	590.2357	-702.9211	-755.4569	0	7.3051	-2.3207
	EP5	-827.68106	-	45.8024	-4.9522	-	-839.3139	0	-	-0.9446
	EP6	-591.1848	-	500.0315	-589.4956	-	-676.5325	0	-	2.6232
	EP7	-0.8160	-	-	-827.5289	-	-	0	-	-
	EP8	580.4943	-	-	-601.01	-	-	0	-	-
	EP1	457.3498	-55.2932	727.7665	714.8407	782.2196	409.4026	-18.8291	0.4879	-6.5485
	EP2	-549.0237	-272.4717	-315.4729	-613.5990	-826.2246	780.2082	-3.3027	-23.095	1.188
	EP3	-	189.8737	-832.2260	-	-829.3074	97.9041	-	9.1388	4.3232
58	EP4	-	608.9576	-370.5562	-	-613.9183	-755.4569	-	26.1960	-2.3207
	EP5	-	-	45.8024	-	-	-839.3139	-	-	-0.9446
	EP6	-	-	500.0315	-	-	-676.5325	-	-	2.6232
	EP1	633.8789	380.6651	727.7665	541.7277	746.1343	409.4026	-7.3869	-8.2262	-6.5485
	EP2	-445.7528	91.8670	-315.4729	711.4279	835.8591	780.2082	4.4122	-4.2978	1.188
	EP3	-793.8439	-810.0667	-832.2260	267.1015	168.0367	97.9041	6.3119	13.7431	4.3232
1,605	EP4	-449.8457	435.5296	-370.5562	-712.9423	-738.3894	-755.4569	-1.6929	14.1097	-2.3207
	EP5	79.7848	-	45.8024	-837.3549	-	-839.3139	-0.1608	-	-0.9446
	EP6	531.6543	-	500.0315	-653.7339	-	-676.5325	3.5349	-	2.6232
	EP1	725.5291	706.4588	727.7665	413.5104	445.7504	409.4026	-6.6046	-6.3393	-6.5485
	EP2	-313.4405	-347.1177	-315.4729	781.1197	768.4833	780.2082	1.0992	0.3908	1.188
	EP3	-832.3082	-793.3506	-832.2260	97.4148	-272.3168	97.9041	4.2955	0.0522	4.3232
176,415	EP4	-360.5240	-339.4988	-370.5562	-760.3914	-768.3216	-755.4569	-2.3426	-1.6083	-2.3207
	EP5	38.7268	20.9565	45.8024	-839.7914	-838.6060	-839.3139	-1.0074	-0.2412	-0.9446
	EP6	502.7300	660.4981	500.0315	-674.6905	-521.4908	-676.5325	2.6639	3.2589	2.6232
	EP1	727.5220	740.7344	727.7665	409.992	384.4834	409.4026	-6.5463	-6.1739	-6.5485
	EP2	-317.1202	-324.2752	-315.4729	779.6153	776.5818	780.2082	1.2016	1.5368	1.188
	EP3	-832.2780	-826.3189	-832.2260	98.0833	141.4893	97.9041	4.3311	5.3053	4.3232
1,406,146	EP4	-370.1207	-422.3838	-370.5562	-755.7654	-728.5607	-755.4569	-2.3131	-1.2819	-2.3207
	EP5	44.5673	425.5364	45.8024	-839.4693	-725.5426	-839.3139	-0.9484	2.6422	-0.9446
	EP6	500.3570	192.6417	500.0315	-676.4064	-818.3549	-676.5325	2.6228	0.7346	2.6232

Table 3: Coordinates of the EPs for uniform packing, random packing and polyehedron model as a function of the number of SPH-Mas, N_{sph}.

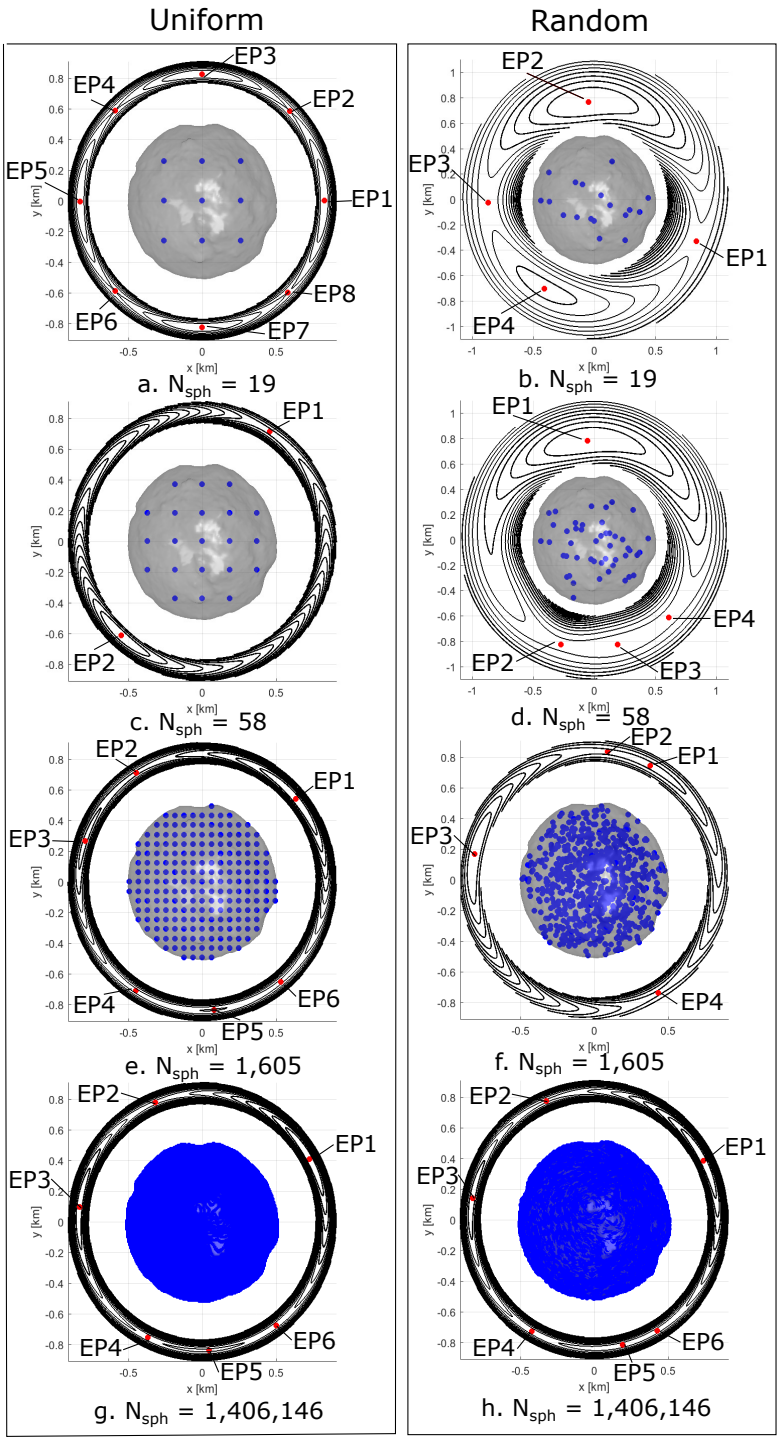

Figure 4: Zero velocity curves and Equilibrium Points (EPs) for the uniform and random packing cases when N_{sph} = 19, 58, 1,605 and 1,406,146.

When keeping μ and ω fixed, the mass distribution plays an important role in the location of the equilibrium points and in their number as shown in the Fig. 4. As a reference, we recall that for a tri-axial ellipsoid at least four EPs exist. For example, Fig. 4.a shows eight EPs similar to the case of a homogeneous cube studied in [31]. When looking at Fig. (4.b), the SPH-Mas are randomly distribute along one direction with four EPs that recalls the case of uniform density elongated asteroids like Eros [26]. This implies that if we are able to detect dust particles around the stable EPs and we can "measure" their locations, we could potentially gain an insights of the mass or density distribution by using Eq. (8). It is highly likely that gravity anomalies exist for asteroids as for the Lunar case [17] and our formula explicitly relate the dynamical properties (EPs) to the distributed density. For the case of symmetric bodies, the EPs are all planar and $\gamma_3 = 0$ as shown in Fig. (2.a) and in Table 3 for the case of uniform sphere packing and $N_{sph} = 19$ or for the tri-axial ellipsoid.

Figure (5) shows the effective potential, the zero velocity curves and the EPs location for the polyhedron model. The equations of the polyhedron potential can be found in [14].

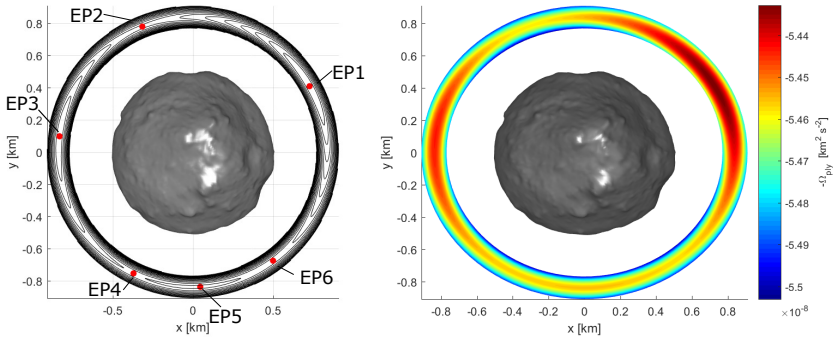

(a) Zero velocity curves and EPs. (b) Effective potential [km^2 s^{-2}]

Figure 5: Polyhedron gravity model: effective potential, zero velocity curves and EPs [32].

The error in the effective potential, Ω, between the uniform SPH-Mas pack-

ing with 1.4 million spheres and the polyhedron model is shown in Fig. 6. The error in Ω is of the order of $O(-12)$ km^2 s^{-2} that corresponds to errors in γ_1, γ_2 and γ_3 between 0.5 m and 1.5 m. Further studies in sphere packing are required for improving the gravity field accuracy. For the scope of our paper, we selected the uniform packing with 1.4 million spheres has SPH-Mas model and we will apply our results to this specific sphere packing throughout the rest of the paper.

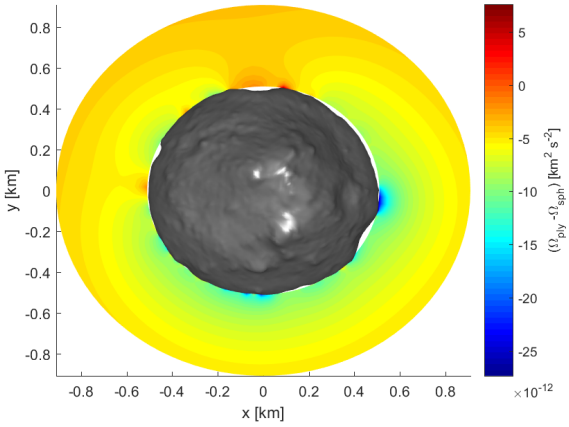

Figure 6: Error in the effective potential Ω between the uniform SPH-Mas with 1.4 million spheres and the polyhedron model.

An important remark is that the sphere packing is highly influenced by the dynamical properties of irregular bodies. Because of our interest in sphere packing, we noticed that most of the literature as been done for hydrodynamic simulations. However, we couldn't find any reference in the impact physics community where the sphere packing is done by preserving the dynamical properties (i.e. EPs coordinate) of irregular bodies. As demonstrated by Raskin and Owen[18], the initial conditions of the sphere packing distribution highly influences the results of hydrodynamic simulations for example the fate of particles when an N-Body simulation is started. As a result of this preliminary

analysis, our recommendation is to select an initial sphere packing condition for hydrodynamic simulations that preserves the gravity properties of the irregular body and not only its polyhedron shape.

4. Linear Equations around the Equilibrium Points for the Mascon Model without the SRP Effect

By adding Eq. (1) to Eq. (6), the effective potential, $\bar{\Omega}$, turns into:

$$\bar{\Omega} = \frac{1}{2}\omega^2(X^2+Y^2) + \sum_{i\,=\,1}^{N_{sph}} \left(\frac{Gm_i}{\boldsymbol{\rho}_i}\right) \tag{9}$$

with $\boldsymbol{\rho}_i = |\boldsymbol{r} - \boldsymbol{r}_i|$ and $|\boldsymbol{\rho}_i|^2 = (X-X_i)^2 + (Y-Y_i)^2 + (Z-Z_i)^2$. We now apply the following change of coordinates to Eq. (5)

$$\begin{cases} X &= x + \gamma_1 \\ Y &= y + \gamma_2 \\ Z &= z + \gamma_3 \end{cases} \tag{10}$$

where γ_1, γ_2 and γ_3 are the positions of the equilibrium points. By applying the change of coordinates, Eq. (5) turns into:

$$\begin{cases} \ddot{x} - 2\omega\dot{y} &= \bar{\Omega}_x \\ \ddot{y} + 2\omega\dot{x} &= \bar{\Omega}_y \\ \ddot{z} &= \bar{\Omega}_z \end{cases} \tag{11}$$

After the change of coordinates, we apply the Taylor expansion as in [27, 11]. The centrifugal term of $\bar{\Omega}$ turns into:

$$\frac{1}{2}\omega^2\left[(x+\gamma_1)^2 + (y+\gamma_2)^2\right], \tag{12}$$

and the potential term of one SPH-Mas (m_i) is

$$\frac{\mu_i}{r_i} = \frac{\mu_i}{\sqrt{(x+\gamma_1-X_i)^2 + (y+\gamma_2-Y_i)^2 + (z+\gamma_3-Z_i)^2}}. \tag{13}$$

We consider the following Taylor expansion up to the second order as in [28]:

$$\begin{aligned} P &= \tfrac{1}{\sqrt{(x-A)^2+(y-B)^2+(z-C)^2}} \\ &= \tfrac{1}{D}\left(1 + \tfrac{Ax+By+Cz}{D^2} + \tfrac{3}{2}\tfrac{(Ax+By+Cz)^2}{D^4} - \tfrac{1}{2}\tfrac{x^2+y^2+z^2}{D^2}\right) \end{aligned} \tag{14}$$

with $D^2 = A^2 + B^2 + C^2$. We also notice that the partial derivatives of P in x, y and z up to the first order are given by

$$\begin{array}{ll} \frac{\partial P}{\partial x} & = \frac{A}{D^3} + \frac{3A(Ax+By+Cz)}{D^5} - \frac{x}{D^3} \\ \frac{\partial P}{\partial y} & = \frac{B}{D^3} + \frac{3B(Ax+By+Cz)}{D^5} - \frac{y}{D^3} \\ \frac{\partial P}{\partial z} & = \frac{C}{D^3} + \frac{3C(Ax+By+Cz)}{D^5} - \frac{z}{D^3}. \end{array} \tag{15}$$

After those considerations, we can recognize that:

$$\frac{\mu_i}{r_i} = \frac{\mu_i}{\sqrt{(x-(X_i-\gamma_1))^2 + (y-(Y_i-\gamma_2))^2 + (z-(Z_i-\gamma_3))^2}} \tag{16}$$

with $A_i = X_i - \gamma_1$, $B_i = Y_i - \gamma_2$, $C_i = Z_i - \gamma_3$ and $D_i^2 = A_i^2 + B_i^2 + C_i^2$. Now we can compute the partial derivatives of $\bar{\Omega}$ in x, y and z. The term in $\bar{\Omega}_x$ is given by:

$$\begin{array}{ll} \bar{\Omega}_x = & \omega^2\gamma_1 + \sum_i^N \mu_i \frac{A_i}{D_i^3} \\ & + \left[\omega^2 + \sum_i^N \mu_i \frac{(3A_i^2 - D_i^2)}{D_i^5}\right] x \\ & + \sum_i^N \mu_i \frac{3A_iB_i}{D_i^5} y \\ & + \sum_i^N \mu_i \frac{3A_iC_i}{D_i^5} z \end{array}, \tag{17}$$

while, the term in $\bar{\Omega}_y$ is:

$$\begin{array}{ll} \bar{\Omega}_y = & \omega^2\gamma_2 + \sum_i^N \mu_i \frac{B_i}{D_i^3} \\ & + \sum_i^N \mu_i \frac{3B_iA_i}{D_i^5} x \\ & + \left[\omega^2 + \sum_i^N \mu_i \frac{(3B_i^2 - D_i^2)}{D_i^5}\right] y \\ & + \sum_i^N \mu_i \frac{3B_iC_i}{D_i^5} z \end{array}. \tag{18}$$

Finally, the term in $\bar{\Omega}_z$ has the form of:

$$\begin{array}{ll} \bar{\Omega}_z = & \sum_i^N \mu_i \frac{C_i}{D_i^3} \\ & + \sum_i^N \mu_i \frac{3C_iA_i}{D_i^5} x \\ & + \sum_i^N \mu_i \frac{3C_iB_i}{D_i^5} y \\ & + \sum_i^N \mu_i \frac{(3C_i^2 - D_i^2)}{D_i^5} z \end{array}. \tag{19}$$

The linear equations of motion around the EPs are derived as:

$$\begin{cases} \ddot{x} - 2\omega\dot{y} &= a_1 x + a_2 y + a_3 z \\ \ddot{y} + 2\omega\dot{x} &= a_2 x + b_2 y + b_3 z \\ \ddot{z} &= a_3 x + b_3 y + c_3 z \end{cases} \tag{20}$$

where the coefficients a, b, and c depend on μ_i, $\boldsymbol{r}_i$, and ω (we recall also that $\gamma_k = \gamma_k(\mu_i, \boldsymbol{r}_i, \omega)$, $k = 1, 2, 3$) and have the following values:

$$\begin{aligned} a_1 &= \left[\omega^2 + \sum_i^N \mu_i \tfrac{(3A_i^2 - D_i^2)}{D_i^5}\right] \\ a_2 &= \sum_i^N \mu_i \tfrac{3A_i B_i}{D_i^5} \\ a_3 &= \sum_i^N \mu_i \tfrac{3A_i C_i}{D_i^5} \\ b_1 &= \sum_i^N \mu_i \tfrac{3B_i A_i}{D_i^5} \\ b_2 &= \left[\omega^2 + \sum_i^N \mu_i \tfrac{(3B_i^2 - D_i^2)}{D_i^5}\right] , \\ b_3 &= \sum_i^N \mu_i \tfrac{3B_i C_i}{D_i^5} \\ c_1 &= \sum_i^N \mu_i \tfrac{3C_i A_i}{D_i^5} \\ c_2 &= \sum_i^N \mu_i \tfrac{3C_i B_i}{D_i^5} \\ c_3 &= \sum_i^N \mu_i \tfrac{(3C_i^2 - D_i^2)}{D_i^5} \end{aligned} \tag{21}$$

note that $b_1 = a_2$, $c_1 = a_3$ and $c_2 = b_3$ and $A_i = X_i - \gamma_1$, $B_i = Y_i - \gamma_2$, $C_i = Z_i - \gamma_3$ and $D_i^2 = A_i^2 + B_i^2 + C_i^2$. The coefficients of Eq. (21) are a generalise formula for non-uniform irregular shape bodies. When an SPH-Mas distribution is derived from a given order in the spherical haramonics, our formula is not limited to the second order coefficients of the spherical harmonics. This can be explained by the fact that the SPH-Mas can be distributed inside the polyhedron shape to retrieve higher order Stokes coefficients. Therefore, Eq. (21) is a generalised version of [12] when using the equivalent SPH-Mas model. Eq. (20) can be rewritten in a matrix form as:

$$\begin{Bmatrix} \dot{x} \\ \dot{y} \\ \dot{z} \\ \ddot{x} \\ \ddot{y} \\ \ddot{z} \end{Bmatrix} = \begin{bmatrix} 0 & 0 & 0 & 1 & 0 & 0 \\ 0 & 0 & 0 & 0 & 1 & 0 \\ 0 & 0 & 0 & 0 & 0 & 1 \\ a_1 & a_2 & a_3 & 0 & 2\omega & 0 \\ a_2 & b_2 & b_3 & -2\omega & 0 & 0 \\ a_3 & b_3 & c_3 & 0 & 0 & 0 \end{bmatrix} \begin{Bmatrix} x \\ y \\ z \\ \dot{x} \\ \dot{y} \\ \dot{z} \end{Bmatrix}, \tag{22}$$

and its characteristic equation is given by:

$$\Lambda^3 + (4\omega^2 - a_1 - b_2 - c_3)\Lambda^2 + (b_2c_3 + a_1c_3 + a_1b_2 - a_2^2 - b_3^2 - a_3^2 - 4\omega^2c_3)\Lambda + (-a_1b_2c_3 - 2a_3b_3a_2 + a_1b_3^2 + c_3a_2^2 + b_2a_3^2) = 0 \tag{23}$$

the roots of Eq. (23) are solved with analytic formulas as in [33] and are donated by $\lambda_1, \ldots, \lambda_6$.

4.1. Case of the Saddle×Center×Center EP

For the Saddle×Center×Center EP, we have two real roots and four imaginary roots. Therefore, the eigenvalues are of the type $\lambda_{1,2} = \pm\lambda$, $\lambda_{3,4} = \pm\Omega i$ and $\lambda_{4,5} = \pm\nu i$. Taking into account the above discussion on the roots of the characteristic Eq. (23), the solution of the Eq. (20) can be written as:

$$\begin{cases} x = & \alpha_1 e^{\lambda t} + \alpha_2 e^{-\lambda t} + \alpha_3\ c(\Omega t) + \alpha_4\ s(\Omega t) + \alpha_5\ c(\nu t) + \alpha_6\ s(\nu t) \\ y = & \alpha_1 k_1 e^{\lambda t} + \alpha_2 k_2 e^{-\lambda t} + \alpha_3(k\ c(\Omega t) - m\ s(\Omega t)) + \alpha_4(k\ s(\Omega t) + m\ c(\Omega t)) + \\ & \alpha_5(r\ c(\nu t) - s\ s(\nu t)) + \alpha_6(r\ s(\nu t) + s\ c(\nu t)) \\ z = & \alpha_1 q_1 e^{\lambda t} + \alpha_2 q_2 e^{-\lambda t} + \alpha_3(q\ c(\Omega t) + d\ s(\Omega t)) + \alpha_4(q\ s(\Omega t) - d\ c(\Omega t)) + \\ & \alpha_5(p\ c(\nu t) + u\ s(\nu t)) + \alpha_6(p\ s(\nu t) - u\ c(\nu t)) \\ \dot{x} = & \alpha_1 \lambda e^{\lambda t} - \alpha_2 \lambda e^{-\lambda t} - \alpha_3 \Omega\ s(\Omega t) + \alpha_4 \Omega\ c(\Omega t) - \alpha_5 \nu\ s(\nu t) + \alpha_6 \nu\ c(\nu t) \\ \dot{y} = & \alpha_1 k_1 \lambda e^{\lambda t} - \alpha_2 k_2 \lambda e^{-\lambda t} + \alpha_3(-k\Omega\ s(\Omega t) - m\Omega\ c(\Omega t)) + \alpha_4(k\Omega\ c(\Omega t) - m\Omega\ s(\Omega t)) + \\ & \alpha_5(-r\nu\ s(\nu t) - s\nu\ c(\nu t)) + \alpha_6(r\nu\ c(\nu t) - s\nu\ s(\nu t)) \\ \dot{z} = & \alpha_1 q_1 \lambda e^{\lambda t} - \alpha_2 q_2 \lambda e^{-\lambda t} + \alpha_3(-q\Omega\ s(\Omega t) + d\Omega\ c(\Omega t)) + \alpha_4(q\Omega\ c(\Omega t) + d\Omega\ s(\Omega t)) + \\ & \alpha_5(-p\nu\ s(\nu t) + u\nu\ c(\nu t)) + \alpha_6(p\nu\ c(\nu t) + u\nu\ s(\nu t)) \end{cases} \tag{24}$$

and for $j = 1, \ldots, 6$, k_j and q_j are:

$$k_j = \frac{(\lambda_j^2 - c_3)(\lambda_j^2 - a_1) - a_3^2}{(\lambda_j^2 - c_3)(2\omega\lambda_j + a_2) + b_3a_3} \qquad q_j = \frac{(a_3 + b_3k_j)}{(\lambda_j^2 - c_3)} \tag{25}$$

where $k_{1,2}$ are real numbers and $k_{3,4}$ and $k_{5,6}$ are two couple of complex conjugate numbers so that:

$$k = \Re(k_3) = \Re(k_4) \qquad m = \Im(k_3) = -\Im(k_4) \tag{26}$$

$$r = \Re(k_5) = \Re(k_6) \qquad s = \Im(k_5) = -\Im(k_6) \tag{27}$$

$$q = \Re(q_3) = \Re(q_4) \qquad d = -\Im(q_3) = \Im(q_4) \tag{28}$$

$$p = \Re(q_5) = \Re(q_6) \qquad u = -\Im(q_5) = \Im(q_6) \tag{29}$$

Eq. (24) can be rewritten in a matrix form as:

$$\begin{Bmatrix} x \\ y \\ z \\ \dot{x} \\ \dot{y} \\ \dot{z} \end{Bmatrix} = \begin{bmatrix} e^{\lambda t} & e^{-\lambda t} & c(\Omega t) & s(\Omega t) & c(\nu t) & s(\nu t) \\ k_1 e^{\lambda t} & k_2 e^{-\lambda t} & (k\ c(\Omega t) - m\ s(\Omega t)) & (k\ s(\Omega t) + m\ c(\Omega t)) & (r\ c(\nu t) - s\ s(\nu t)) & (r\ s(\nu t) + s\ c(\nu t)) \\ q_1 e^{\lambda t} & q_2 e^{-\lambda t} & (q\ c(\Omega t) + d\ s(\Omega t)) & (q\ s(\Omega t) - d\ c(\Omega t)) & (p\ c(\nu t) + u\ s(\nu t)) & (p\ s(\nu t) - u\ c(\nu t)) \\ \lambda e^{\lambda t} & -\lambda e^{-\lambda t} & -\Omega\ s(\Omega t) & \Omega\ c(\Omega t) & -\nu\ s(\nu t) & \nu\ c(\nu t) \\ k_1 \lambda e^{\lambda t} & -k_2 \lambda e^{-\lambda t} & (-k\Omega\ s(\Omega t) - m\Omega\ c(\Omega t)) & (k\Omega\ c(\Omega t) - m\Omega\ s(\Omega t)) & (-r\Omega\ s(\Omega t) - s\Omega\ c(\Omega t)) & (r\Omega\ c(\Omega t) - s\Omega\ s(\Omega t)) \\ q_1 \lambda e^{\lambda t} & -q_2 \lambda e^{-\lambda t} & (-q\Omega\ s(\Omega t) + d\Omega\ c(\Omega t)) & (q\Omega\ c(\Omega t) + d\Omega\ s(\Omega t)) & (-p\Omega\ s(\Omega t) + u\Omega\ c(\Omega t)) & (p\Omega\ c(\Omega t) + u\Omega\ s(\Omega t)) \end{bmatrix} \begin{Bmatrix} \alpha_1 \\ \alpha_2 \\ \alpha_3 \\ \alpha_4 \\ \alpha_5 \\ \alpha_6 \end{Bmatrix} \tag{30}$$

4.2. Case of the Center×Center×Center EP

For the Center×Center×Center EP, we have six imaginary roots. Therefore, the eigenvalues are of the type $\lambda_{1,2} = \pm\eta i$, $\lambda_{3,4} = \pm\Omega i$ and $\lambda_{4,5} = \pm\nu i$. Taking into account the above discussion on the roots of the characteristic Eq. (23),

the solution of the Eq. (20) can be written as:

$$\begin{cases} x = & \alpha_1\ c(\eta t) + \alpha_2\ s(\eta t) + \alpha_3\ c(\Omega t) + \alpha_4\ s(\Omega t) + \alpha_5\ c(\nu t) + \alpha_6\ s(\nu t) \\ y = & \alpha_1(e\ c(\eta t) - f\ s(\eta t)) + \alpha_2(e\ s(\eta t) + f\ c(\eta t)) + \\ & \alpha_3(k\ c(\Omega t) - m\ s(\Omega t)) + \alpha_4(k\ s(\Omega t) + m\ c(\Omega t)) + \\ & \alpha_5(r\ c(\nu t) - s\ s(\nu t)) + \alpha_6(r\ s(\nu t) + s\ c(\nu t)) \\ z = & \alpha_1(g\ c(\nu t) + h\ s(\eta t)) + \alpha_2(g\ s(\eta t) - h\ c(\eta t)) + \\ & \alpha_3(q\ c(\Omega t) + d\ s(\Omega t)) + \alpha_4(q\ s(\Omega t) - d\ c(\Omega t)) + \\ & \alpha_5(p\ c(\nu t) + u\ s(\nu t)) + \alpha_6(p\ s(\nu t) - u\ c(\nu t)) \\ \dot{x} = & -\alpha_1\eta\ s(\eta t) + \alpha_2\eta\ c(\eta t) - \alpha_3\Omega\ s(\Omega t) + \alpha_4\Omega\ c(\Omega t) - \alpha_5\nu\ s(\nu t) + \alpha_6\nu\ c(\nu t) \\ \dot{y} = & \alpha_1(-e\eta\ s(\eta t) - f\eta\ c(\Omega t)) + \alpha_2(e\eta\ c(\eta t) - f\eta\ s(\eta t)) + \\ & \alpha_3(-k\Omega\ s(\Omega t) - m\Omega\ c(\Omega t)) + \alpha_4(k\Omega\ c(\Omega t) - m\Omega\ s(\Omega t)) + \\ & \alpha_5(-r\nu\ s(\nu t) - s\nu\ c(\nu t)) + \alpha_6(r\nu\ c(\nu t) - s\nu\ s(\nu t)) \\ \dot{z} = & \alpha_1(-g\eta\ s(\eta t) + h\eta\ c(\eta t)) + \alpha_2(g\eta\ c(\eta t) + h\eta\ s(\eta t)) + \\ & \alpha_3(-q\Omega\ s(\Omega t) + d\Omega\ c(\Omega t)) + \alpha_4(q\Omega\ c(\Omega t) + d\Omega\ s(\Omega t)) + \\ & \alpha_5(-p\nu\ s(\nu t) + u\nu\ c(\nu t)) + \alpha_6(p\nu\ c(\nu t) + u\nu\ s(\nu t)) \end{cases} \tag{31}$$

and for $j = 1, \ldots, 6$, k_j and q_j are given in Eq. (25) where $k_{1,2}$, $k_{3,4}$ and $k_{5,6}$ are three couple of complex conjugate numbers so that:

$$e = \Re(k_1) = \Re(k_2) \qquad f = \Im(k_1) = -\Im(k_2) \tag{32}$$

$$g = \Re(q_1) = \Re(q_2) \qquad h = -\Im(q_1) = \Im(q_2) \tag{33}$$

Eq. (31) organised in a matrix form is:

$$\begin{Bmatrix} x \\ y \\ z \\ \dot{x} \\ \dot{y} \\ \dot{z} \end{Bmatrix} = \begin{bmatrix} c(\eta t) & s(\eta t) & c(\Omega t) & s(\Omega t) & c(\nu t) & s(\nu t) \\ (e\ c(\eta t) - f\ s(\eta t)) & (e\ s(\eta t) + f\ c(\eta t)) & (k\ c(\Omega t) - m\ s(\Omega t)) & (k\ s(\Omega t) + m\ c(\Omega t)) & (r\ c(\nu t) - s\ s(\nu t)) & (r\ s(\nu t) + s\ c(\nu t)) \\ (g\ c(\eta t) + h\ s(\eta t)) & (g\ s(\eta t) - h\ c(\eta t)) & (q\ c(\Omega t) + d\ s(\Omega t)) & (q\ s(\Omega t) - d\ c(\Omega t)) & (p\ c(\nu t) + u\ s(\nu t)) & (p\ s(\nu t) - u\ c(\nu t)) \\ -\eta\ s(\eta t) & \eta\ c(\eta t) & -\eta\ s(\eta t) & \Omega\ c(\Omega t) & -\nu\ s(\nu t) & \nu\ c(\nu t) \\ (-e\eta\ s(\eta t) - f\eta\ c(\eta t)) & (e\eta\ c(\eta t) - f\eta\ s(\eta t)) & (-k\Omega\ s(\Omega t) - m\Omega\ c(\Omega t)) & (k\Omega\ c(\Omega t) - m\Omega\ s(\Omega t)) & (-r\Omega\ s(\Omega t) - s\Omega\ c(\Omega t)) & (r\Omega\ c(\Omega t) - s\Omega\ s(\Omega t)) \\ (-g\eta\ s(\eta t) + h\eta\ c(\eta t)) & (g\eta\ c(\eta t) + h\eta\ s(\eta t)) & (-q\Omega\ s(\Omega t) + d\Omega\ c(\Omega t)) & (q\Omega\ c(\Omega t) + d\Omega\ s(\Omega t)) & (-p\Omega\ s(\Omega t) + u\Omega\ c(\Omega t)) & (p\Omega\ c(\Omega t) + u\Omega\ s(\Omega t)) \end{bmatrix} \begin{Bmatrix} \alpha_1 \\ \alpha_2 \\ \alpha_3 \\ \alpha_4 \\ \alpha_5 \\ \alpha_6 \end{Bmatrix} \tag{34}$$

As previously mentioned, we selected the uniform packing SPH-Mas with 1.4 million sphere, Fig. (2).g, for testing the analytic formula in Eq. (30) and in Eq. (34). Those formulas relate the amplitudes of the unstable, α_1 (saddle EP), stable, α_2 (saddle EP), and center, $\alpha_{3,\ldots,6}$ ($\alpha_{1,2}$ for center EP), manifolds to the state vector. In our analysis, the amplitudes, α, have a dynamical meaning and are a direct function of the asteroid properties which is different from [15]. Table 4, Table 5 and Table 6 show the value of the eigenvalues evaluated at the EPs and their characteristic time (saddle type, S) or period (center type, C), τ_k and the values of the coefficients in Eq. (21).

		γ_1 [m]	γ_2 [m]	γ_3 [m]	τ_1 [h]	τ_2 [h]	τ_3 [h]
EP1	C	727.5220	409.9917	-6.5463	29.3485	7.9935	7.5551
EP2	S	-317.1202	779.6153	1.2016	±5.1512	7.6516	7.4114
EP3	C	-832.2780	98.0833	4.3311	33.5446	7.9934	7.4971
EP4	S	-370.1207	-755.7654	-2.3131	±8.3984	7.7814	7.4176
EP5	C	44.5673	-839.4693	-0.9484	60.4949	7.8897	7.4551
EP6	S	500.3570	-676.4064	2.6228	±6.7335	7.7251	7.4262

Table 4: Case of uniform packing with 1.4 million SPH-Mas as shown in Fig. (2).g: equilibrium points and period of equilibrium point if of center type (C) or characteristic time if of saddle type (S), τ_k (k = 1,2,3).

		$\lambda \times 10^{-5}$	$\eta \times 10^{-5}$	$\Omega \times 10^{-4}$	$\nu \times 10^{-4}$
EP1	C	-	5.946914872216549	2.183439392554108	2.310126011327043
EP2	S	5.392519079002234	-	2.280993871353600	2.354911317472917
EP3	C	-	5.203015530698535	2.183454198875764	2.327995229682762
EP4	S	3.307519222255295	-	2.242936338236756	2.352951582760225
EP5	C	-	2.885084714416272	2.212152056557068	2.341130896536438
EP6	S	4.125300025347895	-	2.259284765271528	2.350225752251053

Table 5: Case of uniform packing with 1.4 million SPH-Mas as shown in Fig. (2).g: eigenvalues of the equilibrium points.

		$a_1 \times 10^{-7}$	$a_2 \times 10^{-8}$	$a_3 \times 10^{-9}$	$b_3 \times 10^{-10}$	$c_3 \times 10^{-8}$
EP1	C	1.206806509310326	6.753415094923515	1.183996273392401	1.877013611150309	-5.523292682567136
EP2	S	0.220643757809098	-5.670195341165472	-0.490375987257088	-5.183634358626882	-5.642109452721930
EP3	C	1.580517282177134	-1.872410377020379	0.807492207829235	3.147794687604298	-5.646671053744046
EP4	S	0.308858654711669	6.400008301494577	-0.100170237463239	-1.847758376656525	-5.720955066780157
EP5	C	0.007067197283102	-0.866227179537754	0.386004575660976	-1.901323263577832	-5.689989415916555
EP6	S	0.566974014565146	-7.755908950172511	0.043668255858074	3.710365633871921	-5.672624455034453

Table 6: Linearised equation's coefficients of Eq. (21) evaluated in the EPs of the uniform packing with 1.4 million SPH-Mas as shown in Fig. (2).g.

4.3. Planar Equilibrium Points ($\gamma_3 = 0$)

When the EPs are planar and $\gamma_3 = 0$ (i.e, tri-axial ellipsoid), the coefficients a_3 and b_3 of Eq. (22) are zero ($a_3 = b_3 = 0$). Note that we verified that at the EPs $c_3 < 0$, and so the z component behaves as an harmonic oscillator. We can thus compute the characteristic polynomial associate to the (x, y) in-plane motion and then compute the out-of-plane component. The characteristic equation associated to the (x, y) in-plane can be easily obtained as:

$$\Lambda^4 + (4\omega^2 - a_1 - b_2)\Lambda^2 + a_1 b_2 - a_2^2 = 0. \tag{35}$$

with its roots denoted by $\lambda_1, \ldots, \lambda_4$.

For the case of the Saddle×Center×Center EP, the eigenvalues are of the type $\lambda_{1,2} = \pm\lambda$, $\lambda_{3,4} = \pm\Omega i$ and $\lambda_{4,5} = \pm\nu i$. Taking into account the above discussion on the roots of the characteristic Eq. (35) and the uncoupling between the xy and z components, the solution of the Eq. (20) can be written as:

$$\begin{cases} x = & \alpha_1 e^{\lambda t} + \alpha_2 e^{-\lambda t} + \alpha_3\ c(\Omega t) + \alpha_4\ s(\Omega t) \\ y = & \alpha_1 k_1 e^{\lambda t} + \alpha_2 k_2 e^{-\lambda t} + \alpha_3(k_3\ c(\Omega t) + k_4\ s(\Omega t)) + \alpha_4(k_3\ s(\Omega t) - k_4\ c(\Omega t)) \\ z = & \alpha_5\ c(\nu t) + \alpha_6\ s(\nu t) \\ \dot{x} = & \alpha_1 \lambda e^{\lambda t} - \alpha_2 \lambda e^{-\lambda t} - \alpha_3 \Omega\ s(\Omega t) + \alpha_4 \Omega\ c(\Omega t) \\ \dot{y} = & \alpha_1 k_1 \lambda e^{\lambda t} - \alpha_2 k_2 \lambda e^{-\lambda t} + \alpha_3(-k_3 \Omega\ s(\Omega t) + k_4 \Omega\ c(\Omega t)) + \alpha_4(k_3 \Omega\ c(\Omega t) + k_4 \Omega\ s(\Omega t)) \\ \dot{z} = & -\alpha_5 \nu\ s(\nu t) + \alpha_6 \nu\ c(\nu t) \end{cases} \tag{36}$$

with

$$k_1 = \frac{\lambda^2 - a_1}{2\omega\lambda + a_2} \qquad k_2 = -\frac{(\lambda^2 - a_1)}{(2\omega\lambda - a_2)} \tag{37}$$

$$k_3 = \frac{-a_2(\Omega^2 + a_1)}{4\omega^2\Omega^2 + a_2^2} \qquad k_4 = \frac{-2\omega\Omega(\Omega^2 + a_1)}{(4\omega^2\Omega^2 + a_2^2)} \tag{38}$$

Eq. (36) can be rewritten in a matrix form as

$$\begin{Bmatrix} x \\ y \\ \dot{x} \\ \dot{y} \end{Bmatrix} = \begin{bmatrix} e^{\lambda t} & e^{-\lambda t} & c(\Omega t) & s(\Omega t) \\ k_1 e^{\lambda t} & k_2 e^{-\lambda t} & (k_3\ c(\Omega t) + k_4\ s(\Omega t)) & (k_3\ s(\Omega t) - k_4\ c(\Omega t)) \\ \lambda e^{\lambda t} & -\lambda e^{-\lambda t} & -\Omega\ s(\Omega t) & \Omega\ c(\Omega t) \\ k_1\lambda e^{\lambda t} & -k_2\lambda e^{-\lambda t} & (-k_3\Omega\ s(\Omega t) + k_4\Omega\ c(\Omega t)) & (k_3\Omega\ c(\Omega t) + k_4\Omega\ s(\Omega t)) \end{bmatrix} \begin{Bmatrix} \alpha_1 \\ \alpha_2 \\ \alpha_3 \\ \alpha_4 \end{Bmatrix} \tag{39}$$

and

$$\begin{Bmatrix} z \\ \dot{z} \end{Bmatrix} = \begin{bmatrix} c(\nu t) & s(\nu t) \\ -\nu\ s(\nu t) & \nu\ c(\nu t) \end{bmatrix} \begin{Bmatrix} \alpha_5 \\ \alpha_6 \end{Bmatrix}. \tag{40}$$

To prevent repetition in our paper, we leave to the reader to derive the formulation for the case of the Center×Center×Center EP when $\gamma_3 = 0$.

5. Application to Ryugu Asteroid

In this section, we apply the derived Eq. (30) and Eq. (34) formulas to the asteroid Ryugu. The properties of Ryugu are summarised in Table 1. We use the sphere packing presented in Fig. (2).g for the SPH-Mas gravity model. We find 15 families (C1-C15) of POs around the 1:1 resonances of Ryugu. Figure (7-9) shows a 3D, (x,z) and (y,z) views of the family of POs near the EPs. The states are related with the amplitudes, α, in a linear time-dependent form (Eq. (30) and Eq. (34)) and Fig. (7-9) are obtained by fixing the amplitudes at the values listed in Table 7.

So far, we have shown a methodology for analytic constructions of POs about the EPs when the gravity field is modelled with SPH-Mas. Eq. (30-34) holds true for any irregular shape bodies and density distribution. We applied those formulas for studying the linear dynamics of the asteroid Ryugu. We demonstrated that SPH-Mas, if properly packed inside the body shape, can

capture important dynamical properties of the asteroid as equilibrium points and periodic orbits.

Family	EPs		α_1	α_2	α_3	α_4	α_5	α_6
C1	EP1	C	[0.1-0.4]	[0.1-0.4]	0	0	0	0
C2	EP1	C	0	0	[0.15-0.3]	[0.15-0.3]	0	0
C3	EP1	C	0	0	0	0	[0.15-0.3]	[0.15-0.3]
C4	EP2	S	0	0	[0.1-0.4]	[0.1-0.4]	0	0
C5	EP2	S	0	0	0	0	[0.1-0.4]	[0.1-0.4]
C6	EP3	C	[0.05-0.2]	[0.05-0.2]	0	0	0	0
C7	EP3	C	0	0	[0.05-0.2]	[0.05-0.2]	0	0
C8	EP3	C	0	0	0	0	[0.05-0.2]	[0.05-0.2]
C9	EP4	S	0	0	[0.1-0.4]	[0.1-0.4]	0	0
C10	EP4	S	0	0	0	0	[0.1-0.4]	[0.1-0.4]
C11	EP5	C	[0.1-0.4]	[0.1-0.4]	0	0	0	0
C12	EP5	C	0	0	[0.1-0.4]	[0.1-0.4]	0	0
C13	EP5	C	0	0	0	0	[0.1-0.4]	[0.1-0.4]
C14	EP6	S	0	0	[0.1-0.4]	[0.1-0.4]	0	0
C15	EP6	S	0	0	0	0	[0.1-0.4]	[0.1-0.4]

Table 7: Selected amplitudes values for the center EP (C) and saddle EP (S).

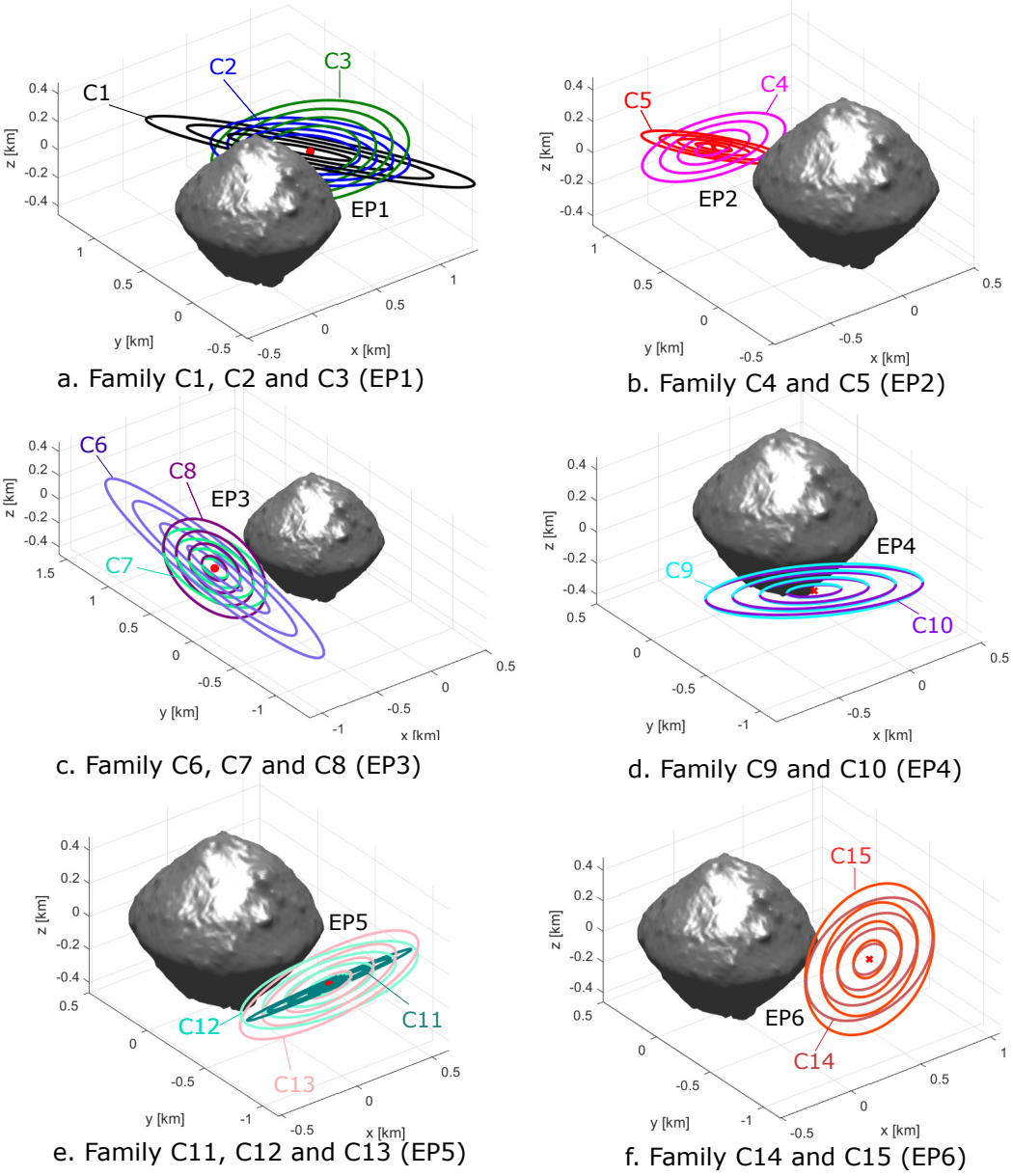

Figure 7: Family of Periodic Orbits (POs) around the 1:1 resonances by using Eq. (30) and Eq. (34) for the SPH-Mas model of Fig. (2).

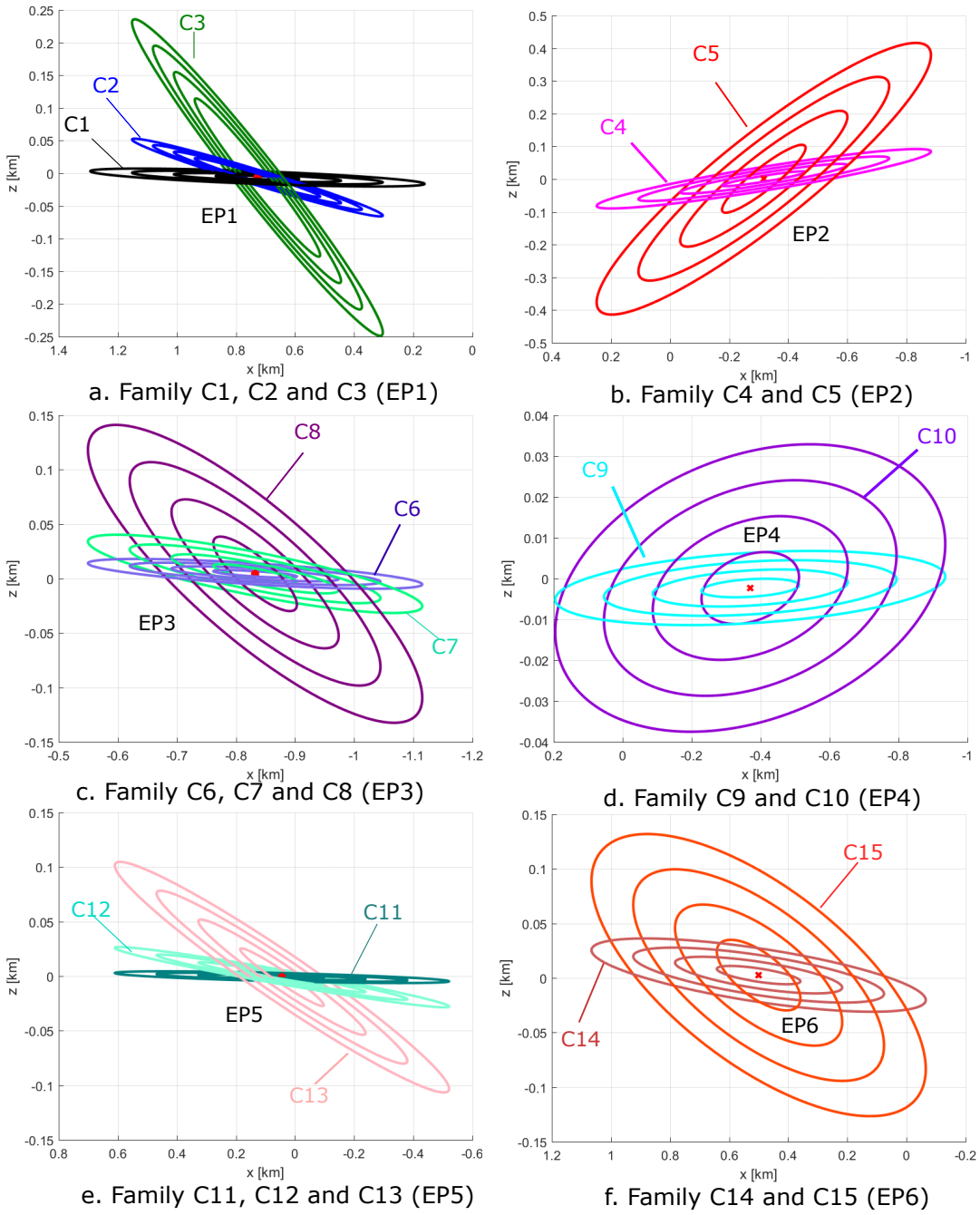

Figure 8: Family of Periodic Orbits (POs) around the 1:1 resonances by using Eq. (30) and Eq. (34) for the SPH-Mas model of Fig. (2): (x,z) view.

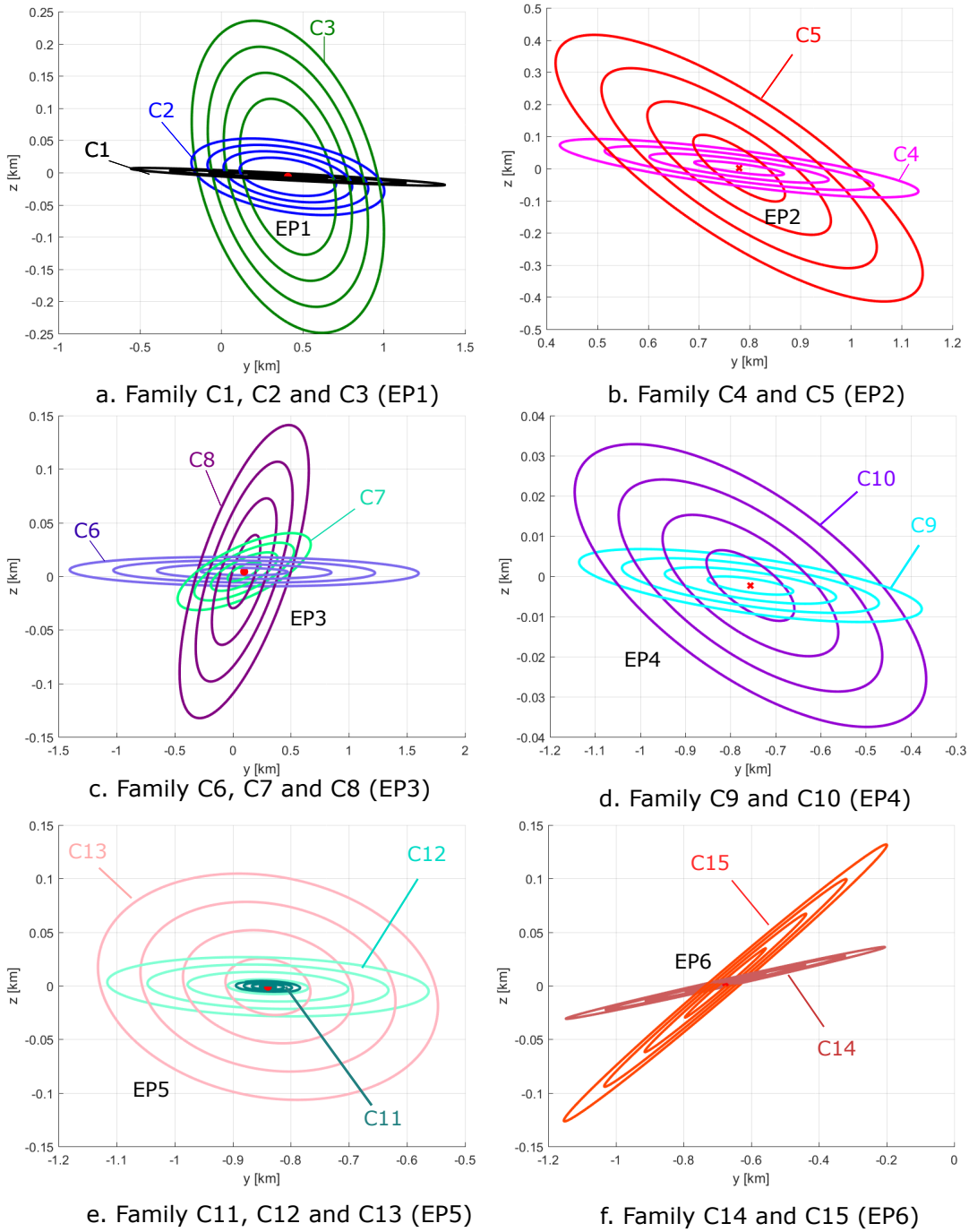

Figure 9: Family of Periodic Orbits (POs) around the 1:1 resonances by using Eq. (30) and Eq. (34) for the SPH-Mas model of Fig. (2): (y,z) view.

6. Hayabusa2's Small Carry-on Impactor Operation

In this section, the case scenario of the Hayabusa2's Small Carry-on Impactor (SCI) operation [6] is investigated. By using the formulation in Eq. (30-34), we gained insights into the dynamics around EPs when the effect of SRP is not taken into account. We make use of a direct numerical approach where the ejetca initial conditions are integrated in high-fidelity. When the SRP effect is included, Eq. (5) becomes time-dependent and generally EPs no longer exist [34]. However, particles can still be temporary captured for several months as for asteroid P/2010 A2 [7]. This fact might suggests the existence of dynamical substitutes as for the restricted three body problem [35]. Considering the time span of the SCI operation (two weeks), it is possible that some particles might stay in orbit and potentially damage the spacecraft. Figure 10 shows the escape trajectory for Hayabusa2 spacecraft in the Home Position (HP) reference frame.

The escape trajectory was designed following the requirement to place the spacecraft behind Ryugu during the explosion. This choice was made to naturally shield the spacecraft from any high-speed debris produced at SCI explosion. Moreover, the spacecraft was required to maintain few kilometres relative distance with DCAM3 for two hours after the impact event. During those hours, data transfer from DCAM3 to the spacecraft occurred. For further details in the escape trajectory deign, refer to Saiki et al [6] In the HP reference frame, the Z_{HP} is along the Asteroid-Earth line pointing towards the Earth. The Sun-Asteroid line belong to the positive coordinates of the (X_{HP}, Z_{HP}) plane while the Y_{HP} axis is defined as for a right handed coordinate system. Table 8 shows the epoch of the escape trajectory for each trajectory legs. The relative distance between the spacecraft's and the particles is monitored to record possible collisions during the simulation.

LEG	Initial Epoch	Final Epoch
1	2019/04/05 00:00:00 UTC	2019/04/05 00:39:60 UTC
2	2019/04/05 00:39:60 UTC	2019/04/05 05:18:20 UTC
3	2019/04/05 05:18:20 UTC	2019/04/20 05:18:20 UTC

Table 8: Epoch of the escape trajectory.

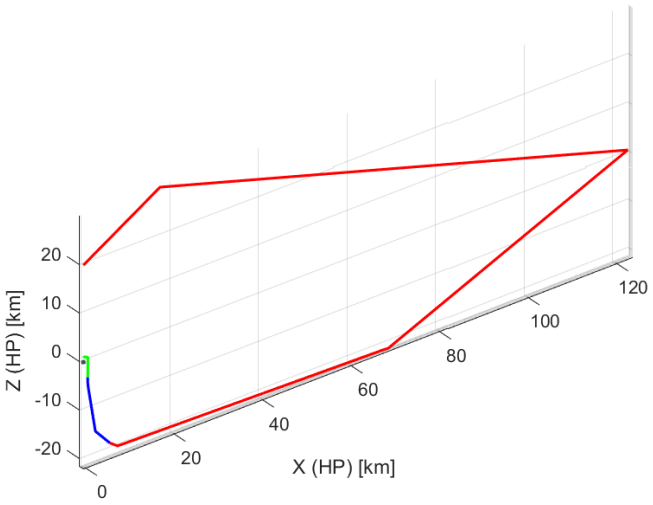

Figure 10: Hayabusa2 Escape Trajectory: Leg1 (green), Leg2 (blue) and Leg3 (red).

6.1. Initial Conditions of Ejecta Particles

The crater size and particles launch speed are given through the ejecta scaling laws that are empirical, but based on dimensional analysis, found from experimental studies [36]. The scaling law provides the velocity distribution of ejecta particles along the crater radius as shown in Fig. 11. The maximum radius of the crater formed by SCI was expected to be 5 m, based on a scaling law on the impact crater size. Taking into account the boulder-rich surface of Ryugu [37], we assumed the crater radius to be less than 5 m. We recall that

for the two-body problem, the escape velocity of Ryugu is $V_{ej} = \sqrt{\frac{\mu}{r_B}} = 0.38$ m s^{-1}. Therefore, we expect that only particles close to the edge of the crater can potentially orbiting Ryugu. For the nominal case, the ejecta is expected to be launched at 45° as shown in Fig. (11). In Figure (11), a is the projectile radius, R is the crater radius around 2 m, v is the particle ejection speed, $n_1 = 1.2$ and $n_2 = 1$ are non-dimensional parameters depending on the material properties of the projectile and the target. Note that we integrate the trajectories of particles with coordinate x within $n_1 a \leq x \leq n_2 R$. We use goNEAR tool (gravitational orbit Near Earth Asteroid Regions) for high-fidelity integration of the dynamics. goNEAR tool was developed and tested in real time during the operations of Hayabusa2's solar conjunction phase [38]. It accounts of the (1) polyhedron gravity perturbation, (2) solar radiation pressure, (3) solar tides and (4) other planets perturbation. goNEAR is written in J2000EQ, therefore the ejecta curtain, which is an assemblage of ejecta particles forming an inverse conical shape and looks like a "curtain", is first given in a local horizon (LH) frame, moved to asteroid fixed frame and finally to J2000EQ as shown in Fig. 12. The nominal impact point is at 300° longitude and 20° latitude.

6.2. Fate of Ryugu's Ejecta: Preparation to the SCI Operation

In preparation to the SCI operation, we selected 3,000 points in the crater's area of radius 2 m. Each point is representative of an ejecta particle with speed distribution shown in Fig. (11). We repeated the simulation four times by changing the diameter of the particles (10 cm, 5 cm, 1 cm and 1 mm) for a total of 12,000 trajectories integrated with goNEAR. The reflectivity coefficient of the particle, $(1 + \rho)$ in Eq. (7), was assumed equal to 1.1. Table 9 summarizes the result of the simulation. We classify the trajectories in three categories: (a) Escape Trj. for those particles that experience an unbounded motion from Ryugu, (b) Impact Trj. for the particles that re-impact on the asteroid surface and (c) Orbit for those particles that have a bounded motion around Ryugu. As one can see, less than 1% of the trajectories analysed can survive into orbit spacecraft for particle diameters of 5-10 cm. From the numerical experiment,

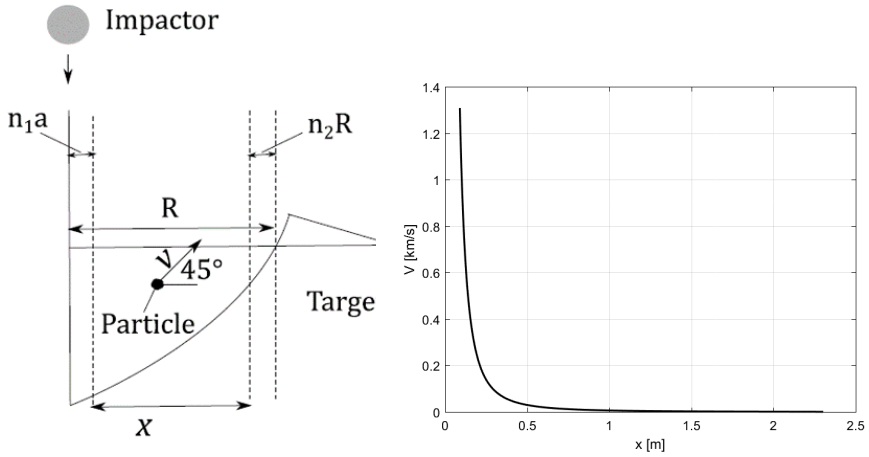

(a) Crater Model: the impact is assumed to be perpendicular to the asteroid surface.

(b) Ejecta initial launch speed as a function of the horizontal distance x from the crater center.

Figure 11: Crater model and ejecta launch speed velocity as function of coordinate x along the radius.

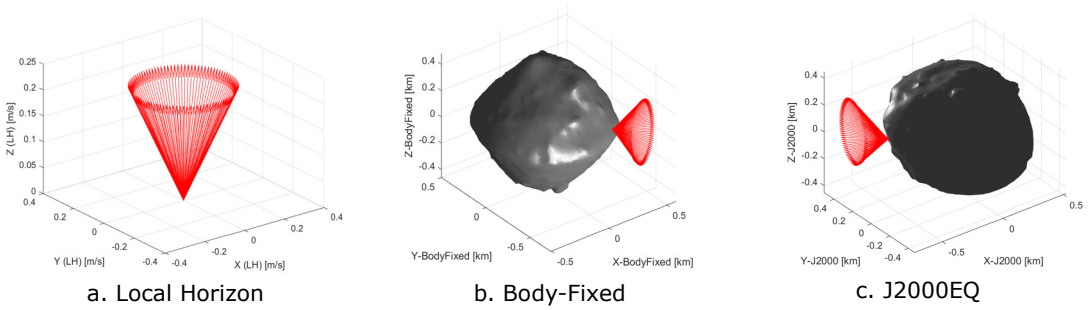

Figure 12: Ejecta curtain initial conditions: Local Horizon, Body-Fixed and J2000EQ .

we couldn't detect any trajectory interference between the spacecraft and the particles which proofs the robustness of the selected escape trajectory. As post-operation evaluation, we couldn't record any damage to the spacecraft from possible particles crossing the spacecraft's trajectory. The process of detecting orbiting particles is still under study.

Figure 14 shows the snapshots of the simulation provided by goNEAR tool.

Most of the particles escape the asteroid gravity, especially mm size particles and high speed particles, while 2% of the particles will impact on Ryugu surface as shown in Fig. (13). Figure (13) shows the longitude, latitude map of the impact point on Ryugu. The yellow square box highlight the SCI impact point. Rows of figures shows the solution for a fixed ejecta diameter. The first column of figures show the impact map and the time of flight of the ejecta. Particles of 1-5 cm have a longer survival than 10 cm particles. The second column shows the impact speed of the particles. As one can notice, some of the particles impact the surface of Ryugu with velocity around or greater than the escape velocity (38 cm s^{-1}) which implies possible re-bouncing dynamics. Last column of the figures gives a qualitative information on where the particles impact on Ryugu and how they are distributed. In the future, we aim to look for evidences of ejecta particles orbiting Ryugu. Ryugu is a relatively "dark" asteroid [2] therefore the effect of SRP onto cm size particles might not affect too much the geometry of the EPs for a short period of time (month scale) and using our linear approximation of Eq. (30-34) can be a good initial guess for the non-linear dynamics.

Dust	Escape Trj.	Impact Trj.	Orbit
10 cm	97.40%	2.53%	0.07%
5 cm	97.44%	2.53%	0.03%
1 cm	97.54%	2.46%	0.00%
1 mm	98.00%	2.00%	0.00%

Table 9: Ejecta particles trajectory probability.

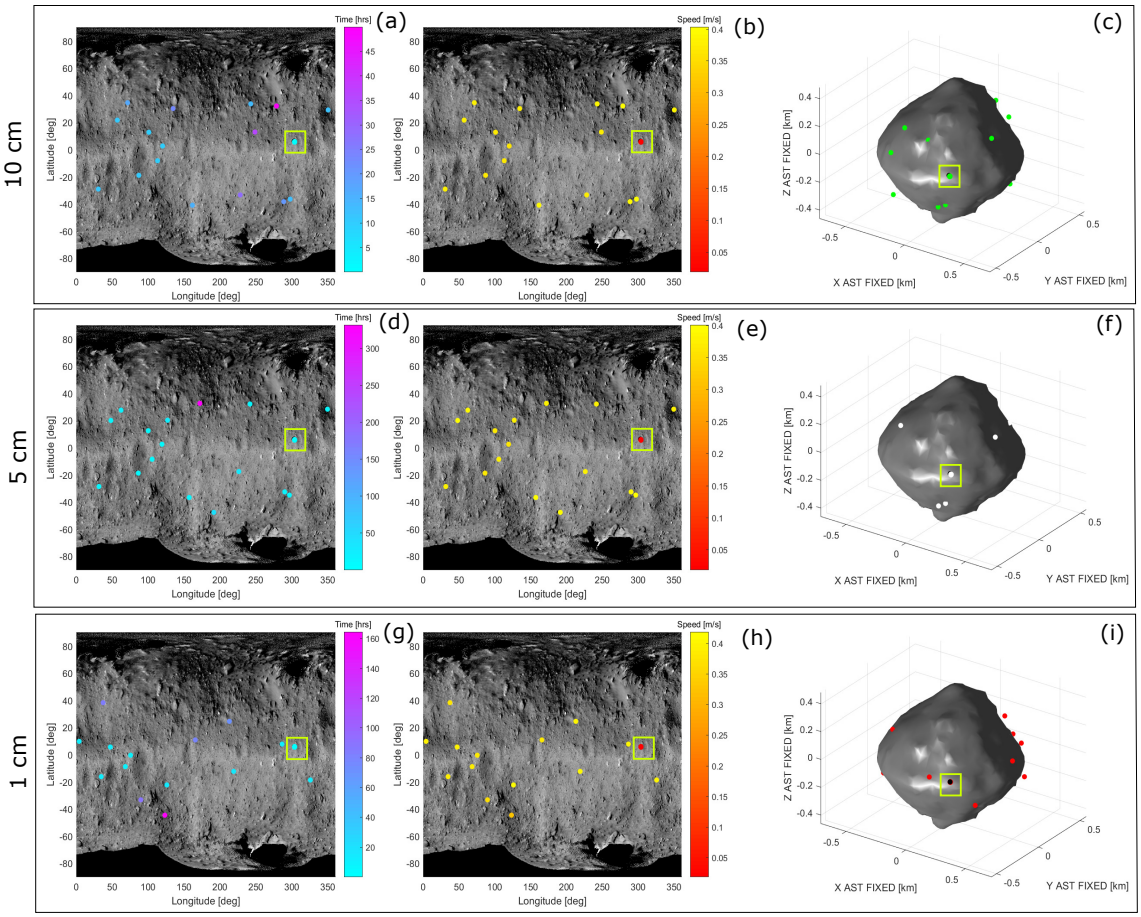

Figure 13: Impact locations of ejecta particles of size 10 cm, 5 cm and 1 cm.

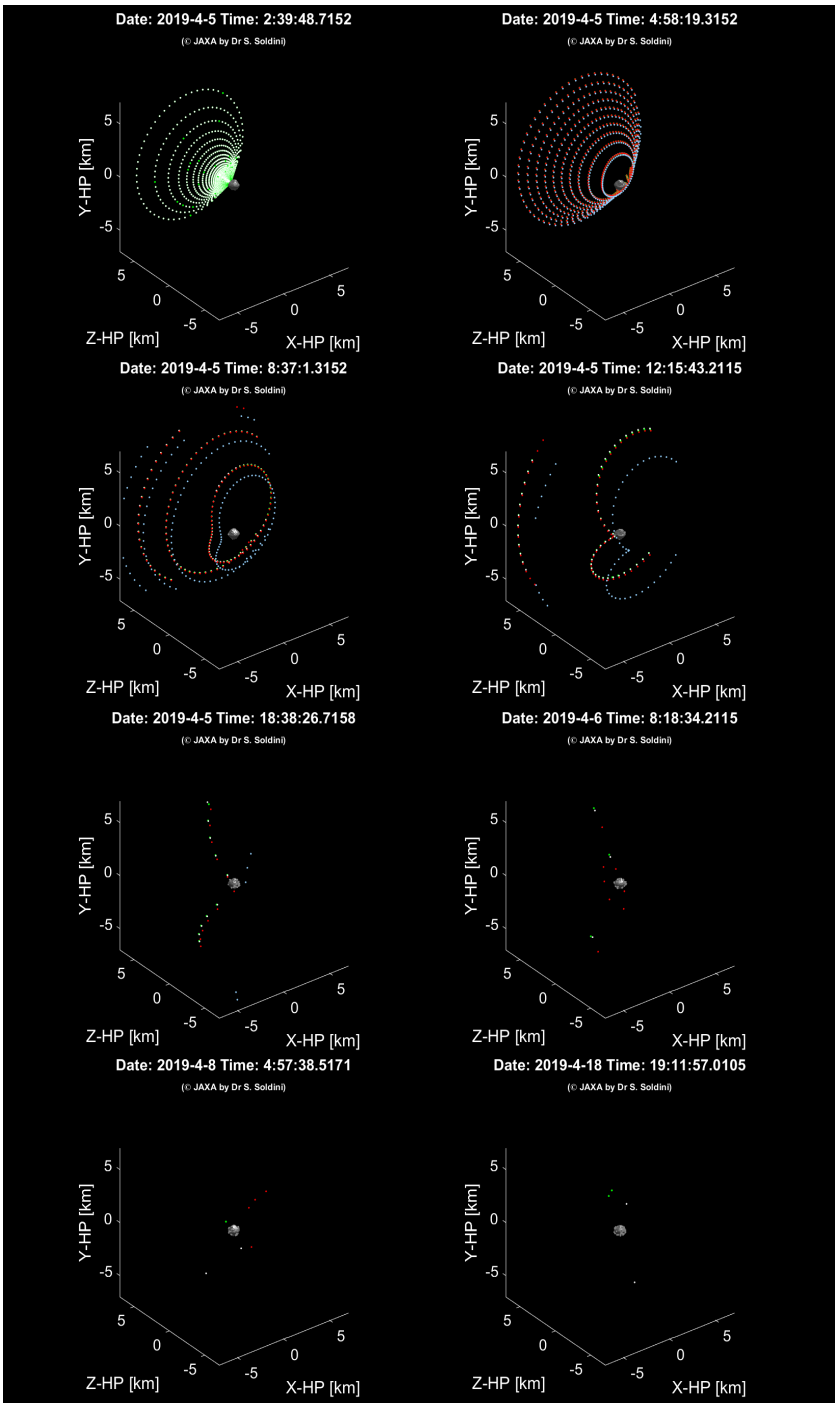

Figure 14: goNEAR tool simulation of Ryugu's ejecta particles: 10 cm (green), 5 cm (white), 1 cm (red) and 1 mm (blue) .

7. Conclusions

In this paper, we presented a methodology to construct analytic solution around the 1:1 resonances of Ryugu. We use the mascon model gravity field to find a linear approximation of the dynamical objects as equilibrium points and periodic orbits. We verify the proposed methodology to the case of the asteroid Ryugu. We compared to SPH-Mas packing and we understood the importance of sphere packing in preserving dynamical objects. The SPH-Mas model has the advantage (1) to be computationally a fast method (we used matrix operation in Matlab to avoid for loops). (2) It allows a semi-analytical formulation of the linearised equations of motion which are derived in this paper. The multi-point mass model also adds the flexibility (3) to give information of the internal mass or density distribution, and (4) to provide a common mesh for SPH codes and astrodynamics tools through a SPH-Mascon gravity model. Our methodology shows that the dynamics of the problem can be preserved with the SPH-Mas model and therefore the SPH-Mas distribution could be potentially used as initial sphere distribution for the SPH astrophysics codes.

Finally, we selected Hayabusa2's SCI impact scenario for studying the dynamics of the ejecta in a non-linear sense. We made use of goNEAR tool to simulate the dynamics of 10 cm, 5 cm, 1 cm and 1 mm in diameter size particles under the effect of the solar radiation pressure perturbation. In the numerical experiment, few particles seem to survive in orbit for diameter of 5-10 cm. The search for evidence of particles in Ryugu orbit is currently a work in progress. We demonstrated that the spacecraft's selected escape trajectory is robust and no collision with particles was detected which has been confirmed by real time operation.

References

[1] S. Watanabe, M. Hirabayashi, N. Hirata, R. Noguchi, Y. Shimaki, H. Ikeda, E. Tatsumi, M. Yoshikawa, S. Kikuchi, H. Yabuta, T. Nakamura, S. Tachibana, Y. Ishihara, T. Morota, K. Kitazato, N. Sakatani, K. Matsumoto, K. Wada, H. Senshu, C. Honda, T. Michikami, H. Takeuchi, T. Kouyama, R. Honda, S. Kameda, T. Fuse, H. Miyamoto, G. Komatsu, S. Sugita, T. Okada, N. Namiki, M. Arakawa, M. Ishiguro, M. Abe, R. Gaskell, E. Palmer, O. S. Barnouin, P. Michel, A. S. French, J. W. McMahon, D. J. Scheeres, P. A. Abell, Y. Yamamoto, S. Tanaka, K. Shirai, M. Matsuoka, M. Yamada, Y. Yokota, H. Suzuki, K. Yoshioka, Y. Cho, S. Tanaka, N. Nishikawa, T. Sugiyama, H. Kikuchi, R. Hemmi, T. Yamaguchi, N. Ogawa, G. Ono, Y. Mimasu, K. Yoshikawa, T. Takahashi, Y. Takei, A. Fujii, C. Hirose, T. Iwata, M. Hayakawa, S. Hosoda, H. S. O. Mori2, T. Shimada, S. Soldini, H. Yano, R. Tsukizaki, M. Ozaki, Y. Iijima, K. Ogawa, M. Fujimoto, T.-M. Ho, A. Moussi, R. Jaumann, J.-P. Bibring, C. Krause, F. Terui, T. Saiki, S. Nakazawa, Y. Tsuda, Hayabusa2 observations of the top-shape carbonaceous asteroid 162173 ryugu, Scienece 364 (6437) (2019) 268–272. doi:10.1126/science.aav8032.

[2] S. Sugita, R. Honda, T. Morota, S. Kameda, H. Sawada, E. Tatsumi, M. Yamada, C. Honda, Y. Yokota, T. Kouyama, N. Sakatani, K. Ogawa, H. Suzuki, T. Okada, N. Namiki, S. Tanaka, Y. Iijima, K. Yoshioka, M. Hayakawa, Y. Cho, M. Matsuoka, N. Hirata, N. Hirata, H. Miyamoto, D. Domingue, M. Hirabayashi, T. Nakamura, T. Hiroi, T. Michikami, P. Michel, R.-L. Ballouz, O. S. Barnouin, C. M. Ernst, S. E. Schröder, H. Kikuchi, R. Hemmi, G. Komatsu, T. Fukuhara, M. Taguchi, T. Arai, H. Senshu, H. Demura, Y. Ogawa, Y. Shimaki, T. Sekiguchi, T. G. Müller, A. Hagermann, T. Mizuno, H. Noda, K. Matsumoto, R. Yamada, Y. Ishihara, H. Ikeda, H. Araki, K. Yamamoto, S. Abe, F. Yoshida, A. Higuchi, S. Sasaki, S. Oshigami, S. Tsuruta, K. Asari, S. Tazawa, M. Shizugami, J. Kimura, T. Otsubo, H. Yabuta, S. Hasegawa, M. Ishiguro, S. Tachibana,

E. Palmer, R. Gaskell, L. Le Corre, R. Jaumann, K. Otto, N. Schmitz, P. A. Abell, M. A. Barucci, M. E. Zolensky, F. Vilas, F. Thuillet, C. Sugimoto, N. Takaki, Y. Suzuki, H. Kamiyoshihara, M. Okada, K. Nagata, M. Fujimoto, M. Yoshikawa, Y. Yamamoto, K. Shirai, R. Noguchi, N. Ogawa, F. Terui, S. Kikuchi, T. Yamaguchi, Y. Oki, Y. Takao, H. Takeuchi, G. Ono, Y. Mimasu, K. Yoshikawa, T. Takahashi, Y. Takei, A. Fujii, C. Hirose, S. Nakazawa, S. Hosoda, O. Mori, T. Shimada, S. Soldini, T. Iwata, M. Abe, H. Yano, R. Tsukizaki, M. Ozaki, K. Nishiyama, T. Saiki, S. Watanabe, Y. Tsuda, The geomorphology, color, and thermal properties of ryugu: Implications for parent-body processes, Science 364 (6437). doi:10.1126/science.aaw0422.

[3] D. S. Lauretta, A. E. Bartels, M. A. Barucci, E. B. Bierhaus, R. P. Binzel, W. F. Bottke, H. Campins, S. R. Chesley, B. C. Clark, B. E. Clark, E. A. Cloutis, H. C. Connolly, M. K. Crombie, M. Delbo, J. P. Dworkin, J. P. Emery, D. P. Glavin, V. E. Hamilton, C. W. Hergenrother, C. L. Johnson, L. P. Keller, P. Michel, M. C. Nolan, S. A. Sandford, D. J. Scheeres, A. A. Simon, B. M. Sutter, D. Vokrouhlicky, K. J. Walsh, The osiris-rex target asteroid (101955) bennu: Constraints on its physical,geological, and dynamical nature from astronomical observations, Meteoritics Planetary Science 50 (4) (2015) 834849. doi:10.1111/maps.12353.

[4] T. Kubota, T. Yoshimitsu, Intelligent rover with hopping mechanism for asteroid exploration, 6th International Conference on Recent Advances in Space Technologies (RAST) (12-14 June 2013) 979–984doi:10.1109/RAST.2013.6581357.

[5] T.-M. Ho, V.Baturkin, C. Grimm, J. T. Grundmann, C. Hobbie, E. Ksenik, C. Lange, K. Sasaki, M. Schlotterer, M. Talapina, N. Termtanasombat, E. Wejmo, L. Witte, M. Wrasmann, G. Wubbels, J. Robler, C. Ziach, R. Findlay, J. Biele, C. Krause, S. Ulamec, M. Lange, O. Mierheim, R. Lichtenheldt, M. Maier, J. Reill, H.-J. Sedlmayr, P. Bousquet, A. Bellion, O. Bompis, C. Cenac-Morthe, M. Deleuze, S. Fredon, E. Jurado,

E. Canalias, R. Jaumann, J.-P. Bibring, K. H. Glassmeier, D. Hercik, M. Grott, L. Celotti, F. Cordero, J. Hendrikse, T. Okada, Mascotthe mobile asteroid surface scout onboard the hayabusa2 mission, Space Science Reviews 208 (1-4) (2017) 339374. doi:https://doi.org/10.1007/s11214-016-0251-6.

[6] T. Saiki, H. Imamura, M. Arakawa, K. Wada, Y. Takagi, M. Hayakawa, K. Shirai, H. Yano, C. Okamoto, The small carry-on impactor (sci) and the hayabusa2 impact experiment, Space Science Reviews 208 (1-4) (2017) 165186. doi:https://doi.org/10.1007/s11214-016-0297-5.

[7] C. Snodgrass, C. Tubiana, J.-B. Vincent, H. Sierks, S. Hviid, R. Moissl, H. Boehnhardt, C. Barbieri, D. Koschny, P. Lamy, H. Rickman, R. Rodrigo, B. Carry, S. C. Lowry, R. J. M. Laird, P. R. Weissman, A. Fitzsimmons, S. Marchi, the OSIRIS team, A collision in 2009 as the origin of the debris trail of asteroid p/2010 a2, Nature 467 (2010) 814816. doi:https://doi.org/10.3847/1538-3881/aa75d0.

[8] NASA, Bennu particle ejection event jan. 19, 2019 (2019).
URL https://www.asteroidmission.org/?attachment_id=15595#main

[9] Y. Yu, Orbital Dynamics in the Gravitational Field of Small Bodies, Springer, 2016.

[10] G. Balmino, Gravitational potential harmonics from the shape of an homogeneous body, Celest. Mech. Dyn. Astron. 60 (1994) 331364. doi:https://doi.org/10.1007/BF00691901.

[11] M. Lara, A. Elipe, Periodic orbits around geostationary positions, Celestial Mechanics and Dynamical Astronomy 82 (3) (2002) 285299. doi:10.1023/A:1015046613477.

[12] J. Feng, X. Hou, Dynamics of the equilibrium points in a uniformly rotating second-order and degree gravitational field, The American Astronomical

Society 154 (21) (2017) 114. doi:https://doi.org/10.3847/1538-3881/aa75d0.

[13] M. Ceccaroni, J. Biggs, Analytic perturbative theories in highly inhomogeneous gravitational fields, Icarus 224 (1) (2013) 74–85. doi:http://doi.org/10.1016/j.icarus.2013.01.007.

[14] R. Werner, D. J. Scheeres, Exterior gravitation of a polyhedron derived and compared with harmonic and mascon gravitation representation of asteroid 4769 castalia, Celest. Mech. Dyn. Astron. 65 (3) (1996) 313344. doi:https://doi.org/10.1007/BF00053511.

[15] Y. Jiang, H. Baoyin, J. Li, H. Li, Orbits and manifolds near the equilibrium points around a rotating asteroid, Astrophys Space Sci 349 (2014) 83106. doi:https://doi.org/10.1007/s10509-013-1618-8.

[16] R. Greenberg, W. F.Bottke, M. Nolan, P. Geissler, J.-M. Petit, D. D.Durda, E. Asphaug, J. Head, Collisional and dynamical history of ida, Icarus 120 (1996) 106–118. doi:https://doi.org/10.1006/icar.1996.0040.

[17] H. J. Melosh, A. M. Freed, B. C. Johnson, D. M. Blair, J. C. A. Hanna, G. A. Neumann, R. J. Phillips, D. E. Smith, S. C. Solomon, M. A. Wieczorek, M. T. Zuber, The origin of lunar mascon basins, Science 340 (6140) (2013) 1552–1555. doi:https://doi.org/10.1126/science.1235768.

[18] C. Raskin, J. M. Owen, Rapid optimal sph particle distributions in spherical geometries for creating astrophysical initial conditions, The Astrophysical Journal 820 (2) (2016) 7. doi:10.3847/0004-637X/820/2/102.

[19] R. Ballouz, K. J. Walsh, D. C. Richardson, P. Michel, Simulations of asteroid reaccumulation: Improving the sph to n-body handoff using alpha shapes, 49th Lunar and Planetary Science Conference, March 19–23 , The Woodlands, Texas, 2018.

[20] A. Colagrossi, Coupled dynamics around irregularly-shaped bodies with enhanced gravity field modelling, Master's thesis, Politecnico di Milano, Milan, Italy (2014).

[21] T. G. G. Chanut, S. Aljbaae, V. Carruba, Dynamics in the vicinity of (101955) bennu: Solar radiation pressure effects in equatorial orbits, Monthly Notice of the Royal Astronomical Society 450 (2015) 37423749. doi:10.1093/mnras/stv845.

[22] P. T. Wittick, R. P. Russell, Mascon models for small body gravity fields, AIAA/AAS Astrodynamics Specialist Conference, 2017.

[23] A. Srinivas, R. Weller, G. Zachmann, Fast and Accurate Simulation of Gravitational Field of Irregular-shaped Bodies using Polydisperse Sphere Packings, in: R. W. Lindeman, G. Bruder, D. Iwai (Eds.), ICAT-EGVE 2017 - International Conference on Artificial Reality and Telexistence and Eurographics Symposium on Virtual Environments, The Eurographics Association, 2017. doi:10.2312/egve.20171361.

[24] S. Tardivel, The limits of the mascons approximation of the homogeneous polyhedron, AIAA/AAS Astrodynamics Specialist Conference, 2016doi:https://doi.org/10.2514/6.2016-5261.

[25] R. P. Russel, N. Arora, Global point mascon models for simple, accurate, and parallel geopotential computation, Journal of Guidance Control and Dynamics 35 (5) (2012) 15681581. doi:https://doi.org/10.2514/1.54533.

[26] T. Fukushima, Precise and fast computation of the gravitational field of a general finite body and its application to the gravitational study of asteroid eros, The Astronomical Journal 154 (145) (2017) 15. doi:https://doi.org/10.3847/1538-3881/aa88b8.

[27] D. L. Richardson, Analytic construction of periodic orbits about the

collinear points, Celestial Mechanics 22 (3) (1980) 241253. doi:https://doi.org/10.1007/BF01229511.

[28] S. Soldini, J. J. Masdemont, G. Gmez, Dynamics of solar radiation pressure-assisted maneuvers between lissajous orbits, Journal of Guidance, Control, and Dynamics 42 (4) (2019) 769–793. doi:10.2514/1.G003725.

[29] J. Burkardt, Matlab function ball_grid.m (2010).
URL http://people.sc.fsu.edu/~%20jburkardt/

[30] S. Holcombe, Matlab function inpolyhedron.m (2016).
URL https://jp.mathworks.com/matlabcentral/fileexchange/37856-inpolyhedron-are-points-inside-a-triangulated-volume

[31] P. Dirac, The lorentz transformation and absolute time, Physica 19 (1-12) (1953) 888–896. doi:10.1016/S0031-8914(53)80099-6.

[32] D. Scheeres, J. W. M. Mahon, A. French, D. Brack, S. Soldini, N. Baresi, H. Ikeda, Y. Tsuda, D. S. Lauretta, T. O.-R. TEAM, Comparing the dynamical environments of bennu and ryugu, ISTS, 15-21 June, Fukui, Japan, 2019.

[33] M. R. Spigel, S. Lipschutz, J. Liu, Schaum's outline of mathematical handbook of formulas and tables, 2013.

[34] X. Xin, D. J. Scheeres, X. Hou, Forced periodic motions by solar radiation pressure around uniformly rotating asteroids, Celestial Mechanics and Dynamical Astronomy 126 (4) (2016) 405–432. doi:10.1007/s10569-016-9701-4.

[35] G. Gómez, J. J. Masdemont, J. M. Mondelo, Dynamical substitutes of the libration points for simplified solar system models, 2003.

[36] K. A. Holsapple, K. R. Housen, A crater and its ejecta: An interpretation of deep impact, Icarus 191 (2, Supplement) (2007) 586 – 597, deep Impact

at Comet Tempel 1. doi:https://doi.org/10.1016/j.icarus.2006.08.035.

[37] K. Wada, M. Grott, P. Michel, K. J. Walsh, A. M. Barucci, J. Biele, J. Blum, C. M. Ernst, J. T. Grundmann, B. Gundlach, A. Hagermann, M. Hamm, M. Jutzi, M.-J. Kim, E. Kührt, L. Le Corre, G. Libourel, R. Lichtenheldt, A. Maturilli, S. R. Messenger, T. Michikami, H. Miyamoto, S. Mottola, T. Müller, A. M. Nakamura, L. R. Nittler, K. Ogawa, T. Okada, E. Palomba, N. Sakatani, S. E. Schröder, H. Senshu, D. Takir, M. E. Zolensky, International Regolith Science Group (IRSG) in Hayabusa2 project, Asteroid ryugu before the hayabusa2 encounter, Progress in Earth and Planetary Science 5 (1) (2018) 82. doi:10.1186/s40645-018-0237-y.

[38] S. Soldini, T. Yamaguchi, Y. Tsuda, S. Takanao, Hayabusa2 mission solar conjunction operation, ISTS, 15-21 June, Fukui, Japan, 2019.